Characterization of S-palmitoylation dependent protein localization by hyperplexed spatial proteomics

By Marijke Stokkel

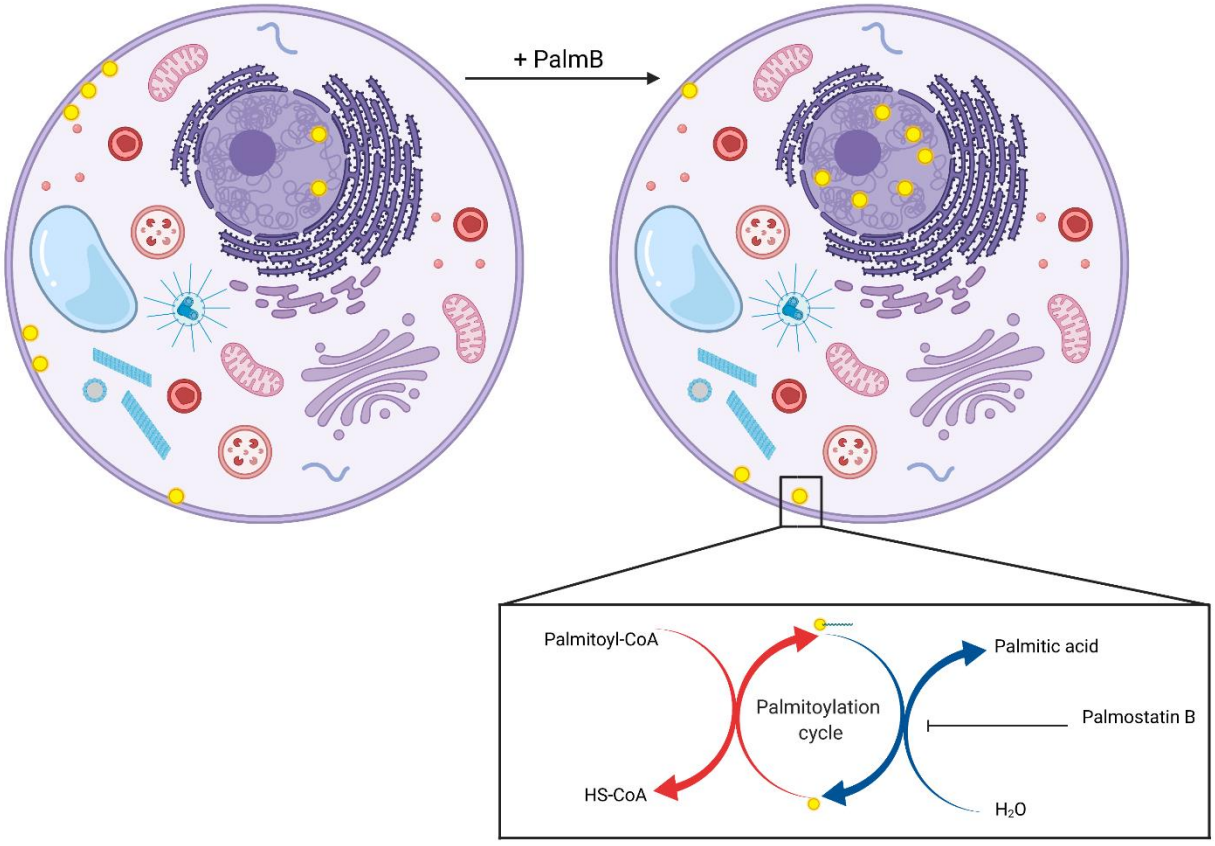

Inhibition of depalmitoylation by Palmostatin B leads to changes in protein localization.

6 December 2021

Supervisor: Dr. Marc Baggelaar
Second examiner: Dr. Joost Sneijder
Second supervisor: PhD candidate Samiksha Sardana

Abstract

S-Palmitoylation is a post translational modification (PTM) associated with numerous cancers and neurological diseases. It is a reversible type of lipidation defined by the addition of a palmitic acid to a cysteine residue. Regulation of this PTM depends on the activity of palmitoyl S-acyl transferases and palmitoyl thioesterases which add and remove the palmitoyl moiety, respectively. S-palmitoylation can have various effects on proteins, of which a change in intracellular localization is most substantiated. While methods for large scale identification of palmitoylated proteins have become well established, the characterization of S-palmitoylation dependent translocations has so far only been studied on a single protein basis. This study aimed to identify S-palmitoylation dependent translocating proteins. The broad spectrum depalmitoylase inhibitor Palmostatin B (PalmB) was employed in combination with differential centrifugation based spatial proteomics to determine translocating proteins. In addition, SILAC-TMT hyperplexing was used to allow for the combined quantitation of treatment groups and spatial proteomics fractions. Using this method we identified 48 potentially translocating proteins. A high overrepresentation of S-palmitoylated proteins was observed among the translocators indicating that the translocation of these enriched proteins may have occurred in response to a change in palmitoylation. Additionally, a STRING database search found many interacting proteins within this group suggesting that some translocations may occur as a result of the translocation of a binding partner. We demonstrate that spatial proteomics can be used as a hypothesis-generating method to identify potential S-palmitoylation dependent translocating proteins. These potential translocators can be used as a starting point for further study into S-palmitoylation dependent protein localization.

Samenvatting

S-palmitoylatie is een eiwitmodificatie waarbij een palmitinezuur, een soort vetzuur, is verbonden aan een cysteïne aminozuur. Deze modificatie wordt gereguleerd door enzymen die de verbinding tussen het palmitinezuur en het eiwit kunnen maken en verbreken. Hierdoor is deze modificatie reversibel. Het toevoegen van een palmitinezuur aan een eiwit heet palmitoylering en het verwijderen van het palmitinezuur heet depalmitoylering. De toevoeging van dit vetzuur aan een eiwit maakt het eiwit meer hydrofoob waardoor het makkelijker kan interacteren met de verschillende membranen van de cel. Als gevolg hiervan kunnen eiwitten die gepalmitoyleerd worden van lokalisatie in de cel veranderen. Deze regulering van eiwitlokalisatie is heel belangrijk in de cel en misregulatie van dit mechanisme kan tot uiteenlopende ziektes leiden. Zo is een verandering van eiwit S-palmitoylatie in verband gebracht met ziektes zoals Alzheimer, Huntington, ALS en kanker.

Voor dit onderzoek is geprobeerd om eiwitten te identificeren die van lokalisatie binnen de cel veranderen als gevolg van een verandering in palmitoylatie. Hiervoor werden humane cellen behandeld met een stof die de enzymen verantwoordelijk voor het verwijderen van palmitinezuren remt. Vervolgens werd gekeken naar het effect van deze remmer op de eiwitlokalisatie met een methode genaamd ‘spatial proteomics’. Voor deze methode werden de organellen van de cel gescheiden in verschillende fracties op basis van toenemende dichtheid door middel van centrifugatie. Daarna werd de eiwitsamenstelling van deze fracties bepaald. Met deze samenstellingen werd een computer algoritme getraind om de scheidingspatronen van organellen te herkennen aan de hand van marker eiwitten waarvan de intracellulaire lokalisatie bekend is. Op deze manier kon de intracellulaire eiwitlokalisatie worden bepaald. Door de centrifugatie neerslagpatronen van eiwitten te vergelijken van cellen behandeld met remmer en zonder remmer konden translokaliserende eiwitten worden geïdentificeerd.

In dit onderzoek werden 48 eiwitten gevonden die mogelijk van lokalisatie in de cel veranderen na behandeling met een depalmitoylatie remmer. Door deze eiwitten te vergelijken met een database van gepalmitoyleerde eiwitten weten we dat 70% van deze mogelijk verplaatsende eiwitten gepalmitoyleerd zijn. In vergelijking met het totaal aan menselijke eiwitten is dat erg veel, aangezien van 20% van de menselijke eiwitten is gevonden dat ze gepalmitoyleerd kunnen worden. Daarnaast liet een database zoekopdracht zien dat een groot deel van de translokaliserende eiwitten met elkaar kunnen interacteren. Dit doet vermoeden dat sommige translokaliserende eiwitten misschien niet individueel verplaatsen, maar samen met hun interactiepartner. We kunnen niet met zekerheid stellen dat deze 48 eiwitten verplaatsen door een verandering in hun palmitoylatie. Desalniettemin suggereert het grote aandeel gepalmitoyleerde eiwitten binnen deze groep wel dat er een link is. Meer onderzoek is nodig naar de link tussen palmitoylatie en eiwit lokalisatie van deze 48 geïdentificeerde eiwitten.

Introduction

S-palmitoylation is a post translational modification (PTM) associated with numerous types of cancers and neurodegenerative diseases[1,2]. S-palmitoylation is the covalent attachment of palmitic acid to a cysteine residue by a thioester linkage. The attachment of the fatty acid is catalyzed by protein acyl transferases (PATs), of which 23 have been identified in mammals[3]. These PATs contain a zinc finger domain and a cysteine rich domain with a DHHC motif and are commonly referred to as zDHHCs. Aside from palmitate, zDHHCs are also capable of transferring other types of fatty acids, in which case the PTM is referred to as S-acylation. S-acylation, including S-palmitoylation, is unique as it is the only type of protein lipidation that is reversible (Fig. 1). Removal of the S-palmitoyl moiety is facilitated by acyl protein thioesterases (APTs), a subset of the serine hydrolase (SH) protein family also referred to as depalmitoylases. Among others, serine hydrolases that have been proven to have depalmitoylase activity include: palmitoyl-protein thioesterase 1 (PPT1), alpha-beta hydrolase domain containing protein 17 (ABHD17), acyl protein thioesterase 1 (APT1) and acyl protein thioesterase 2 (APT2)[4].

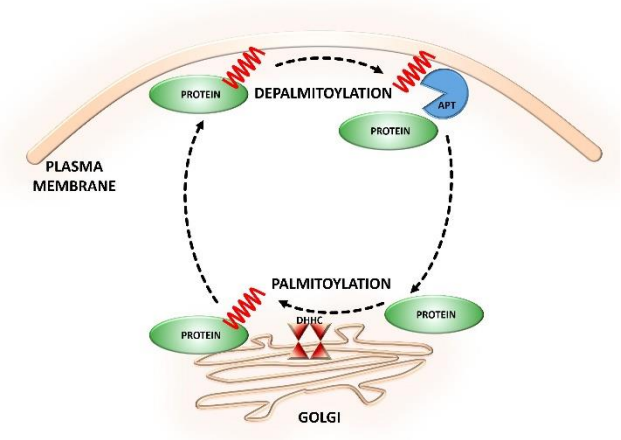

Figure 1. S-palmitoylated proteins can undergo dynamic cycles of palmitoylation and depalmitoylation. PATs in the Golgi catalyze the addition of palmitic acid to cysteine residues of the substrate protein. APTs at the plasma membrane hydrolyze the removal of palmitic acid. Taken from Zaręba-Koziol et al.[2]

S-palmitoylation can alter protein activity and function. This can be accomplished, among others, by changing a protein's conformation or stability, by changing its protein interactors, or by altering the effects of other PTMs. A prime example of palmitoylation affecting protein conformation is the palmitoylation of GPCRs at the cytoplasmic tail, which can result in the formation of a new loop[5]. Palmitoylation has also been shown to change helix structures in amino acid peptide hormones leading to different denaturation behavior under thermal stress[6]. Similarly, palmitoylation can alter protein stability, as is seen for the palmitoylation of SNARE protein Tlg1, which has been shown to prevent ubiquitination and proteasomal degradation[7]. Aside from protein degradation, the interplay between palmitoylation and ubiquitination has also been shown to regulate protein folding. Namely, for Wnt signaling co-receptor LRP6, palmitoylation of the folded protein is required to allow ER exit, which is inhibited by ubiquitination[8]. Additionally, S-palmitoylation can also interact with phosphorylation, as is seen for the co-regulation of transport capacity of dopamine transporter. Here, high phosphorylation combined with low palmitoylation is associated with reduced transport capacity, while low

phosphorylation with high palmitoylation is associated with increased transport capacity[9]. Lastly, S-palmitoylation can promote protein-protein interactions. This can occur either directly, by association of the palmitate moieties, or indirectly, by clustering of S-palmitoylated proteins in membrane microdomains[10].

Not only does S-palmitoylation affect protein function, the palmitoylation state of a protein can also alter its intracellular localization (Fig. 2). H-Ras and PSD-95 for instance, have been shown to relocalize from the plasma membrane to the Golgi and endosomes respectively upon depalmitoylation[11,12]. In fact many proteins, including neurotransmitter receptor GABAR and GPCR β-adrenergic receptor[13,14], depend on S-palmitoylation as a localization signal for expression at the plasma membrane. Similarly, S-palmitoylation has been shown to accelerate the transport of newly translated proteins from cis- to trans-Golgi[15]. This has been proposed to be a result of protein concentration in highly curved regions of the Golgi cisternae, caused by the adoption of a conical shape[15].

Changes in membrane and organellar association mediated by S-palmitoylation are likely the result of altered physicochemical properties. Firstly, the addition of palmitic acid, or any fatty acid, leads to an increase in hydrophobicity, which can enable the association of proteins to lipid rafts and membrane microdomains[16–19]. This may explain the enrichment of S-palmitoylated proteins in ceramide rich lipid rafts[20]. Amyloid precursor protein (APP) is one such proteins that is enriched at lipid rafts upon S-palmitoylation. This enrichment is associated with increased amyloid-β protein processing in Alzheimer's disease[21]. Additionally, it has been proposed that palmitoylation may induce tilting of transmembrane domains (TMD)[22,8] potentially resulting in realignment of transmembrane proteins and allowing for interaction between non-membrane bound S-palmitoylated proteins and membrane proteins.

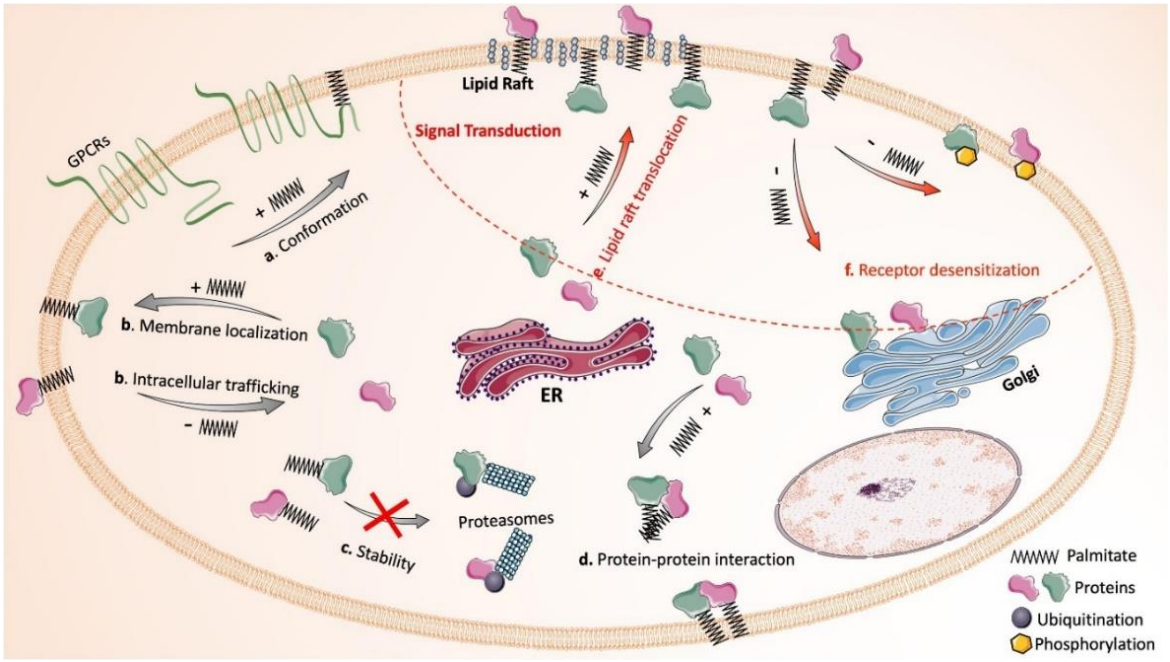

Figure 2. The S-palmitoylation state of a protein affects protein function and localization. (a) The palmitoylation of the cytoplasmic tail of a GPCR can lead to the formation of a new loop. (b) Protein palmitoylation facilitates membrane association and functions in intracellular trafficking. (c) Palmitoylation can reduce protein ubiquitination preventing protein degradation. (d) Palmitoylation regulates protein-protein interactions via direct interaction of fatty acid tails, or indirectly by increasing

proximity within the membrane. (e) Palmitoylation of membrane proteins enables lipid raft association. (f) Depalmitoylation of GPCRs increases accessibility of phosphorylation sites to kinases. Taken from Yang *et al*.[23]

Over the past twenty years considerable progress has been made in the research into S-palmitoylation. Techniques such as acyl-biotin exchange (ABE), acyl-resin assisted capture (acyl-RAC) and lipid metabolic labelling combined with copper catalyzed azide-alkyne cycloaddition (CuAAC) have enabled the large scale identification of S-palmitoylated proteins[24–26]. These methods rely on labeling and enrichment of the S-palmitoylation sites and have facilitated the identification of a considerable number of S-palmitoylated proteins. Data mining of these S-palmitoylation identification studies has revealed that a large portion of synaptic proteins is S-palmitoylated and that this PTM is associated with cancer and nervous system disorders[27]. Additionally, these large amounts of data have led to the generation of the Swisspalm database, which contains identified and predicted S-palmitoylation sites of thousands of proteins originating from various cell and tissue types, as well as organisms[28,29]. The vast amounts of data generated by S-palmitoylation enrichment studies coupled with the increasing interest in artificial intelligence applications in life sciences has also led to the development of multiple S-palmitoylation site predictors[30–32]. However, to date, no universal consensus sequence for S-palmitoylation has been found[33].

In addition to developing S-palmitoylation enrichment techniques, much research has gone into depalmitoylases and their substrates. Activity based probes like fluorophosphonate (FP), which bind to the depalmitoylase active site, have been used to identify and refine depalmitoylase inhibitors in a method termed activity based protein profiling (ABPP). This has led to the identification of APT1 and APT2 inhibitor ML348 and ML349 as well as the broad spectrum inhibitor Palmostatin B (PalmB)[34–36]. Not only do these inhibitors provide powerful tools to characterize depalmitoylase substrates, they also facilitate the study of S-palmitoylation dependent protein localization. In this manner it was shown that PalmB treatment resulted in increased palmitoylation of exogenously expressed N-Ras, which led to its relocalization to endomembranes in MDCK cells[36]. Methods to study depalmitoylases are still being expanded, the latest addition being fluorescence-based probes for screening depalmitoylase activity in living cells[37].

The development of depalmitoylase inhibitors has been instrumental in the study of S-palmitoylation dependent localization and depalmitoylase substrates. However, where enrichment techniques have enabled the large scale identification of S-palmitoylated proteins and S-palmitoylation sites, the study of S-palmitoylation mediated translocations is still performed on a small scale. This is largely because research into protein localization often relies on time consuming methods like fluorescence microscopy, which is only applicable on a protein-by-protein basis. However, over the last decades spatial proteomics techniques have emerged that allow for large scale determination of intracellular protein localization[38].

In spatial proteomics, a cell lysate is separated into fractions containing completely or partially enriched organelles (Fig. 3). Most often, partial separation is used, which can be achieved by either density gradient centrifugation, or differential centrifugation. These types of separations generate a high number of samples per replicate which can be combined by multiplex approaches such as SILAC, TMT and iTRAQ labeling. Methods like (hyper)-LOPIT utilize density gradient centrifugation combined with TMT labeling[39,40], while LOPIT-DC and dynamic organellar maps (DOM) use differential centrifugation coupled to TMT and/or SILAC labeling[41,42]. The resulting subcellular fractions are then analyzed with

bottom-up proteomics, which generates protein profiles. Next, the profiles of protein markers with known intracellular localizations are used to train a classification algorithm to predict the localization of proteins of unknown localization. This type of localization prediction has been used to map the intracellular spatial proteome of various cells and organisms including HeLa, mouse primary neurons, U2-OS and Arabidopsis thaliana callus[41–44]. Additionally, spatial proteomics is also capable of characterizing protein translocations in response to drug or inhibitor treatment[42].

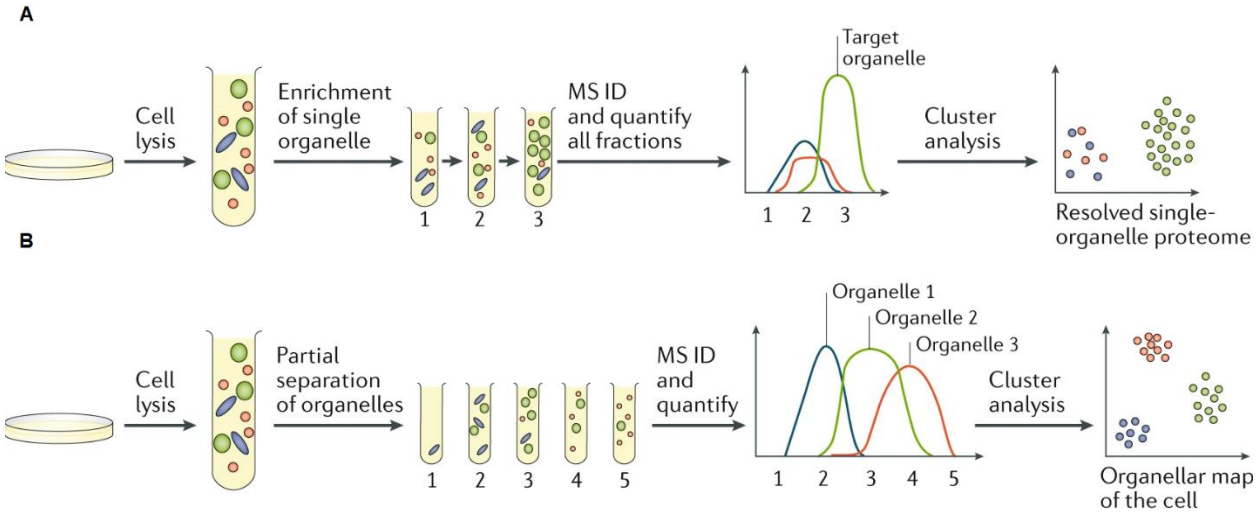

Figure 3. Organelle fractionation coupled to MS analysis allows for spatial proteomics. (A) In single organelle proteomics the target organelle is enriched by subcellular fractionation and the resulting fractions are analyzed with quantitative MS. Protein profiles of contaminants can be distinguished from organelle constituents by statistical analyses. (B) In multi-organelle spatial proteomics, organelles are partially separated followed by quantitative MS. Cluster analysis is used to distinguish organelles based on protein distributions from established organelle markers. Taken from Lundberg and Borner[38].

In this study, we aimed to identify S-palmitoylation mediated translocations on a proteome wide scale. We performed spatial proteomics, using differential centrifugation as the organellar fractionation method, coupled to SILAC-TMT hyperplexing for peptide quantification. Fractionation profiles of protein markers with known localizations were used to train a support vector machine (SVM) to classify proteins of unknown localization. By comparing protein profiles we identified proteins in HEK293T cells that upon treatment with PalmB undergo changes in intracellular protein localization. We found that these potentially translocating proteins are overrepresented in palmitoyl-proteomes compared to the human proteome. However, these translocating proteins have not yet been validated to be S-palmitoylated.

Materials and methods

1. Cell culture

HEK293T cells were maintained in DMEM supplemented with 10% fetal bovine serum (FBS), 2mM L-glutamine, 100 U/mL penicillin and 0.1 mg/mL streptomycin at 37 °C and 5% CO_2. Cells were passaged twice a week, i.e. every 72-96h. Briefly, medium was aspirated and cells were washed with PBS. Cells were detached by incubation with 0.05% trypsin/EDTA for 3-5 min at 37 °C. Fresh medium was added to neutralize the trypsin and the resulting cell suspension was transferred to a centrifuge tube. The cells were spun down at 1200 rpm for 3 min and the cell pellet was resuspended in fresh medium. The cells were split 1:20 or 1:30 depending on the confluence.

For SILAC labeling, cells were grown in heavy or light medium starting at passage 19. Cells were grown for 4 passages, after which the cells were harvested to determine the incorporation efficiency. The remainder of the cells was preserved in cryo-storage prior to expansion for experiments. SILAC heavy medium was prepared by supplementing SILAC DMEM with 100 mg/L $^{13}C_6{}^{15}N_4$- arginine (R10) and $^{13}C_6{}^{15}N_2$-lysine (K8), 10 % dialyzed FBS, 2 mM L-glutamine, 100 U/mL penicillin and 0.1 mg/mL streptomycin. Media was filtered using a 0.22 µM filter and stored at 4 °C. SILAC light medium was prepared identically with an equimolar amount of light arginine (R0, 0.543 mM) and lysine (K0, 0.524 mM).

2. Gel based activity based protein profiling (gel-ABPP)

For *in vitro* ABPP, HEK293T cell pellets (from a T75 flask) were dissolved in 500 µL lysis buffer (50 mM HEPES, 100 mM DTT and 0.5 M $MgCl_2$) and lysed using a probe sonicator (amp 80, 5 pulses, 0.5 sec). Following lysis, 25 units/µL Benzonase® (Millipore, 70746-3) was added and the samples were kept on ice. Protein concentrations were determined with a BCA assay (Thermo Fisher Scientific) and adjusted to 2 mg/mL using lysis buffer. 19 uL of lysate (2 mg/mL) was incubated with 0.5 µL vehicle (DMSO), ML348 (20, 100, 300, 600, 1000 µM) or PalmB (5, 20, 100, 200, 400 µM) inhibitor stocks for 30 min at 37°C while shaking at 700 rpm. The activity based probe FP-TAMRA (Thermo Fisher Scientific) was added to a final concentration of 250 nM and incubated for 30 min at 37°C while shaking at 700 rpm. The labelling reaction was quenched by adding SDS-PAGE sample buffer (Bio-Rad 1610791) with 100 mM DTT. The samples were separated by SDS-PAGE (Criterion™ XT precast gel, 12% Bis-Tris) and visualized by in gel fluorescence scanning (Amersham Imager 600, GE Healthcare, Cy3 channel).

For *in situ* ABPP, 6 well-plate cell cultures were incubated with PalmB at varying concentrations (0, 0.1, 0.3, 1.0, 3.0, 10, 30 µM), or for varying durations (1h, 2h, 3h, 4h). PalmB stocks were prepared in DMSO and diluted in growth medium without FBS. Medium was aspirated and carefully replaced with inhibitor or DMSO supplemented medium. After incubation, the cells were washed gently with PBS and harvested by resuspension in PBS. The cell suspension was spun down at 1200 rpm for 3 min and the pellet was re-solubilized in 100 µL lysis buffer and immediately flash frozen and stored at -80 °C. The following day, the samples were thawed on ice before lysis using a probe sonicator (amp 80, 5 pulses, 0.5 sec). The lysate was adjusted to 2 mg/mL and incubated with 500 nM FP-TAMRA. Identically to the *in vitro* ABPP, the samples were quenched, separated and visualized using SDS-PAGE.

3. Silver stain SDS-PAGE

SDS-PAGE silver stain was used to visualize protein abundance patterns across different fractions generated by differential separation. 0.75 ug protein was diluted in SDS-PAGE sample buffer and separated on a 12% Bis-Tris gel. Gels were fixed in 50% methanol, 12% acetic acid for 1 h followed by washing in 50% methanol for 30 min. After a second wash step in water for 20 min, the gels were sensitized in 0.02% sodiumthiosulphate for 1 min, after which the gels were washed thrice in water for 30 seconds. The gels were incubated in 0.1% silvernitrate at 4 °C for 20 min. Next, the gels were washed thrice in water for 30 seconds and the gel chamber was changed. The silver stain was developed in 3% $NaCO_3$, 0.05% formalin and terminated in 50% methanol, 12% acetic acid. After washing twice for 10 minutes in water, the gels were scanned.

4. Translocation experiment

4.1 Inhibitor incubation

Heavy and Light SILAC labeled cells were incubated with 10 µM PalmB and DMSO respectively for 3 h. As described previously, SILAC medium was prepared, omitting dFBS and supplementing with 10 µM PalmB or DMSO. After incubation, the cells were gently washed with PBS, resuspended in fresh PBS and transferred to a centrifuge tube. The cells were counted by an automated cell counter (Cell Countess 3, Invitrogen) and the heavy and light labeled cells were mixed in a 1:1 ratio. The resulting cell suspensions were centrifuged for 10 min at 200g and 4 °C.

4.2 Lysis and organellar fractionation

Organellar separation was performed by mechanical cells lysis with a ball bearing homogenizer followed by differential centrifugation. Cell pellets were resuspended in 6 mL lysis buffer (50 mM HEPES pH 7.5, 250 mM sucrose, 2mM $MgCl_2$, 2 mM EDTA, EDTA-free Protease Inhibitor Cocktail (cOmplete™, Roche)). Cells were lysed by passaging 1.5 mL of cell suspension 15 times in a ball bearing homogenizer (Isobiotec©) with a 12 µm clearance size. Non-lysed cells and cell debris was pelleted at 200 g for 5 min. The supernatant was subjected to increasing centrifugation speeds (1000g x 10min, 3000g x 10min, 5000g x 10min, 9000g x 15min, 12.000g x 15min, 15.000g x 15min, 30.000g x 20min, 79.000g x 43min and 120.000g x 45min) in an Eppendorf 5920 R centrifuge, a Sorvall RC 6+ centrifuge with F21S rotor or an Optima Max XP centrifuge with MLA-50 rotor. After each centrifugation step, the pellets were washed (50 mM HEPES pH 7.5, 2 mM $MgCl_2$, 2 mM EDTA, 1X protease inhibitors) before being resuspended in buffer (50 mM HEPES pH 8.0, 0.1% Rapigest, 25 units/µL benzonase). Supernatants and pellets were kept on ice during the experiment and flash frozen for storage at -80 °C.

4.3 Peptide sample preparation

The samples were thawed on ice and the protein concentrations were determined using a microBCA assay (ThermoFisher Scientific). Next, the samples were diluted to 0.15 or 0.20 µg/µL (100 µL) with 50 mM HEPES pH 7.5. The proteins were reduced and alkylated by incubation with 5 mM TCEP and 10 mM CAA for 10 min at RT and 600 rpm. LysC was added in a 1:75 enzyme/protein ratio and incubated for 1h at 37 °C at 600 rpm. Samples were trypsinized overnight at 37 °C and 600 rpm with trypsin in a 1:75 ratio.

The following day, the peptide samples were acidified to pH<3 with trifluoroacetic acid (TFA) and desalted using C18 StageTips. Briefly, the columns were activated by washing with 150 µL methanol and

equilibrated by washing with 150 µL proteomics grade H_2O. Samples were spun down for 5 min at 13.000 rpm and loaded onto the columns. The columns were washed with 150 µL H_2O. Lastly, the peptides were eluted by washing the tips with 60 µL 60% acetonitrile. The eluent was collected in LoBind tubes and dried in a centrifugal vacuum concentrator (Labconco, Catalog No. 7310032) and dissolved in 50 mM HEPES pH 8.5.

The different peptide fractions were TMT labeled (Thermo Scientific TMT10plex™) to enable pooling. To prevent condensation, the TMT label reagents were equilibrated to RT before opening. 800 ug TMT labeling reagent was dissolved in 40 µL 100% acetonitrile under occasional vortexing. 200 ug TMT label was used to label 15-20 µg of peptides and incubated for 1h at RT. The labeling reaction was quenched by adding 5% hydroxylamine and incubating 15 min at RT.

After TMT labeling, the peptides were desalted to remove HEPES and unreacted TMT reagent using StageTips, as described earlier. The dried peptides were reconstituted in 2% formic acid and measured on a Q Exactive HF Orbitrap MS instrument to determine purity, signal intensity and TMT labeling efficiency across the fractions. Based on these measurements the fractions were pooled. The 120.000S fraction had a lower signal intensity compared to other fractions. We decided to pool the samples in a volume ratio of 1 for 120.000S to 0.5 for all other fractions.

Peptides were fractionated using offline High pH Reversed-Phase peptide fractionation to lower sample complexity and allow deeper sequencing. 10 mM NH_4OH (pH 10) was used as mobile phase A and a 10 mM NH_4OH, 90% ACN (pH 10) was used as mobile phase B. Peptides were eluted with the following gradient: 0-2% 2min, 2-12% 2-8 min, 12-35 8-55 min, 35-55% 55-62 min, 55-100% 62-65 min, 100-0% 65-105 min with a flow rate of 200 nL/min. Fractions were taken every 60 s and concatenated every 7 fractions resulting in 7 fractions. The samples were dried in a SpeedVac and dissolved in 20 uL 2% FA.

4.4 LC-MS/MS

The peptides were separated and analyzed by nanoLC-MS/MS. Reverse phase chromatography was performed on an UltiMate™ NCS-3500-RS system. For trapping an Acclaim™ PepMap™ 100 C18 HPLC column (5 mm length, 300 µm inner diameter, 5 µm particle size) was used (Thermo Scientific, Cat.no: 160454). The analytical column (50 cm length, 75 µm inner diameter) was packed in house with Poroshell 120 EC-C18 2.7 µm (ZORBAX Chromatographic Packing, Agilent). Column temperature was set to 40°C. Separation was performed with 0.1% formic acid (buffer A) and 80% acetonitrile, 0.1% formic acid (buffer B). Peptides were separated over 115 min with a 300 nL/min flow using buffer B with the following gradient: 0-9% 0-1min, 9-21% 2-97min, 21-45% 97-100min, 45-99% 100-104min, 99-9% 105-115 min.

The LC system was connected to an Orbitrap Exploris 480 via the ESI spray. Full scans were performed at a resolution of 60.000 ppm and a scan range of 375-1600 m/z. The AGC target and the maximum injection time were set to standard and auto mode, respectively. Precursor ions were fragmented with a normalized HCD collision energy of 30%, an isolation window of 1.2 m/z and a resolution of 45000 ppm. The first mass was defined at 120 m/z, the AGC target and maximum injection time were set to standard and auto mode, respectively. The dynamic exclusion was set to 16s with mass tolerance of 10ppm.

4.5 Data processing

Proteome Discoverer (version 2.5.0.400) was used for protein identification using Mascot to search against the UniProt database. Trypsin was set as digestion enzyme with a maximum of 1 allowed missed

cleavage. Precursor mass tolerance and fragment tolerance was set 10ppm and 0.8 Da, respectively. Reporter ions were quantified with a co-isolation threshold of 50 and an average reporter S/N ratio of 10. Peptides and proteins were filtered for 0.01% FDR.

The data was searched independently for heavy and light labeled peptides. For the light search, N-terminal TMT and TMT on lysine were set as dynamic and static modifications, respectively. For the heavy search, N-terminal TMT was set as a dynamic modification, heavy arginine ($^{13}C_6$ $^{15}N_4$) and TMT on heavy lysine ($^{13}C_6{}^{15}N_2$) were set as static modifications. For both searches methionine oxidation and N-terminal acetylation were set as dynamic and cysteine carbamidomethylation was set as static modification. The resulting files containing protein names and TMT quantitation values were filtered for reverse hits and contaminants.

4.6 Translocation

Changes in intracellular protein localization upon inhibitor treatment were quantitatively assessed by calculating the magnitude of translocation, as described by Itzhak *et al*[42]. Normalized protein profiles of inhibitor treated replicates were subtracted from untreated replicates resulting in delta profiles. Outliers of these delta profiles were detected by the squared Mahalanobis distance. Distances to the center of the data were converted to p-values to which multiple hypothesis testing was applied using the Benjamini-Hochberg method. Adjusted p-values were ranked from low to high, multiplied by the protein rank and divided by the total number of proteins generating the Q values. These values where then converted into magnitude scores (-log10(Q) = M).

4.7 Generation of map

The intracellular protein map was generated with the help of the Bioconductor workflow for analyzing spatial proteomics data[45]. This protocol describes how to train a SVM classification algorithm to assign proteins of unknown localization to an intracellular niche based on known marker proteins. We limit the data analysis to supervised machine learning only.

Data was imported into a single MSnSet with Heavy and light denoted as individual replicates and normalized to the sum intensity per protein. Proteins that were not quantified in both heavy and light labeled cells were filtered. Human protein markers present in the pRoloc package were applied to the dataset. Protein markers with an M-score above 0 were not used for training. Organelles with similar marker occupancy profiles were combined and Golgi markers were set to unknown. The support vector machine (SVM) was trained 100 times with a 5-fold cross validation. Class specific weights were set inversely proportional to the number of protein markers mapped per organelle class. Classifier performance was evaluated to determine the optimal sigma and cost for the highest F1 score. A sigma of 0.1, a cost of 16 and the class weights were used for classification. The organelle classification was performed for DMSO and PalmB experiments separately. Organelle specific thresholds were set, below which classification was set to unknown. These thresholds were set at the median prediction score per organelle.

Results

APT1 and APT2 activity in HEK293T lysates.

In order to confirm the presence and activity of APT1 and APT2 in HEK293T cells, a gel-based activity based protein profiling (ABPP) assay was performed. In this ABPP assay, cell lysates or cultures were incubated with PalmB and the remaining enzyme activity was determined by incubation with an activity based fluorescent probe. ML348 and ML349 inhibitors were used to identify bands corresponding to APT1 and APT2, respectively (Sup. Fig. 1 & 2). As can be seen from figure 4A, *in vitro* incubation with PalmB resulted in a four-fold higher inhibition of APT2 than APT1, with an IC_{50} of 0.218 μM and 0.833 μM, respectively. Aside from APT1 and APT2, PalmB also inhibited various other unidentified proteins (Sup. Fig. 3). We attempted to identify these enzymes with an *in situ* proteomics based ABPP. However, results indicated that serine hydrolase enrichment by streptavidin pull-down was unsuccessful (unpublished data). Consequently, no statistically significant inhibition was observed. Although unfortunate, it did not pose a major problem, as in contrast to the *in vitro* inhibition, the *in situ* gel based ABPPs did not indicate that other serine hydrolases were inhibited at concentrations up to 30 μM (Sup. Fig 4).

Optimization of incubation parameters.

In situ ABPP assays were performed to optimize the concentration and duration of PalmB inhibition. Compared to the *in vitro* assay, the IC_{50} of the *in situ* assay was higher for both APT enzymes (Fig. 4B). Similar to the *in vitro* assay, APT2 was more strongly inhibited than APT1. However, this effect was more pronounced in cell culture with a ten-fold difference in IC_{50} of 1.18 μM and 12.3 μM for APT2 and APT1, respectively. A time course experiment was performed to account for the reversible nature of the PalmB inhibitor. At a 10 μM concentration, PalmB exhibited increased inhibition with prolonged incubation times up to 3h, after which the enzyme activity increased again (Fig. 4C). The same concentration range as in figure 4B was re-evaluated with an incubation time of 3h. For these parameters the IC_{50} of both APTs decreased in a similar manner with an approximate factor of 1.5 from 12.3 to 7.93 μM for APT1 and 1.18 to 0.802 μM for APT2. For the translocation experiment cells were incubated with PalmB for 3h at 10 μM to allow for the highest inhibition while minimizing potential off-target effects.

Optimization of lysis method

Spatial proteomics requires a gentle lysis method that leaves the organelles intact for separation. Two mechanical lysis methods, Dounce homogenization and ball-bearing homogenization (Isobiotec), were used to compare the lysis efficiency of HEK293T cells harvested from T175 flasks. The 200 g centrifugation fraction of the Dounce homogenized sample had a higher protein concentration compared to the Isobiotec homogenized samples (Sup. Table I). In contrast, subsequent centrifugation fractions of the Dounce lysate exhibited very low or undetectable protein yields, while the Isobiotec fractions showed detectable protein concentrations in all fractions. This indicates that the Dounce homogenizer is a less efficient lysis method compared to the Isobiotec. This combined with the lower consistency of Dounce homogenization[46] led us to choose the ball-bearing homogenizer as lysis method for our experiment. Lastly, we also tested the Isobiotec homogenizer with balls of different clearance sizes (8, 10 and 12 μm). Protein concentrations of the fractions did not show pronounced differences between different ball sizes (Sup. Table II). More importantly, silver stain SDS-PAGE gels did not show large differences in the protein patterns resolved in the lanes (Sup. Fig. 4). For further experiments we

used a ball with a 12 µm clearance size as this had been used before for mammalian cell lines in spatial proteomics[41].

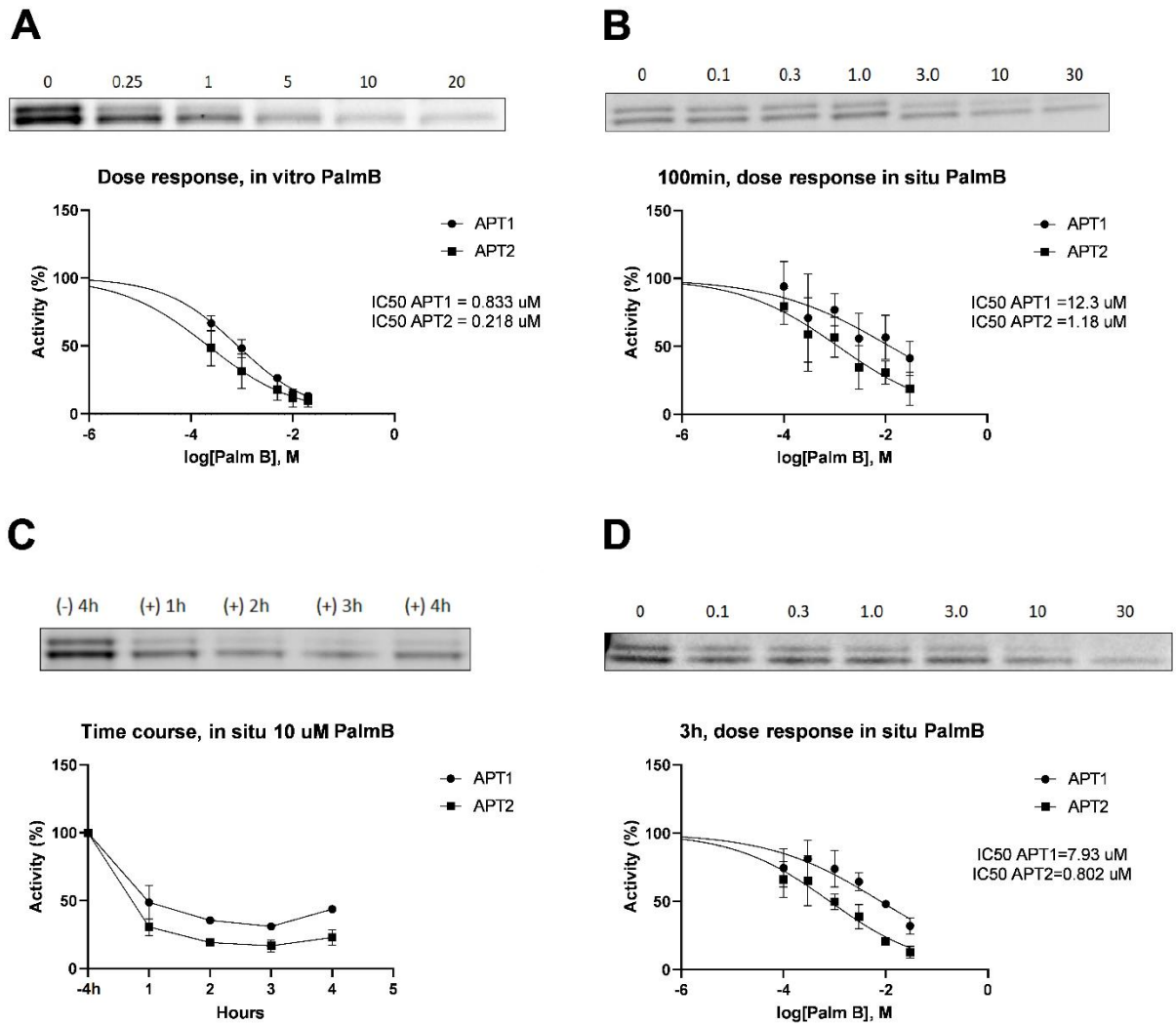

Figure 4. PalmB inhibition of APT1 and APT2. HEK293T cell lysates (A) or cell cultures (B-D) were incubated with PalmB inhibitor or vehicle (DMSO) followed by incubation with FP-TAMRA. Proteins were separated by gel electrophoresis and visualized by fluorescence gel scanning. The percentage inhibition was calculated using fluorescence intensity and normalized to DMSO. (A) *In vitro* inhibition after 30 minutes of inhibitor incubation (0, 0.25, 1, 5, 10, 20 µM). (B, D) *In situ* inhibition after 100 min and 3h, respectively, for an inhibitor concentration range (0, 0.1, 0.3, 1.0, 3.0, 10, 30 µM). (C) *In situ* time course experiment, cells were incubated for 1-4 hours at identical inhibitor concentrations (10 µM) and compared to a 4h incubation without inhibitor (-4h).

Confirmation of organelle separation.

A label free quantification (LFQ) experiment was performed to characterize the organelle separation of a differential centrifugation experiment. Quantitation values were normalized per protein and the resulting profiles were visualized in a PCA plot (Fig. 5A). This plot showed numerous 'lines' of proteins caused by missing values in the same fractions. Furthermore, of the 3421 proteins identified only 607 had fewer than 4 missing values out of the 11 fractions measured. Missing values are a common

problem in label free (spatial) proteomics which will be circumvented in the subsequent translocation experiment by using TMT quantitation. For the current experiment missing values were not imputed for the validation of organelle separation.

Cluster density is visualized in a hexbin plot (Fig. 5B) identifying one particularly dense cluster on the left and a few minor clusters on the right side of the plot. Mapping of protein markers to the data shows that this high-density cluster contains mitochondrial proteins (Fig. 5C). Other well separated clusters include the ribosomes, proteasome and actin cytoskeleton. Other organelles cluster but have overlapping parts including the plasma membrane, endoplasmic reticulum and lysosomes, and the nucleus and cytosol. In contrast, the peroxisomes do not exhibit clustering.

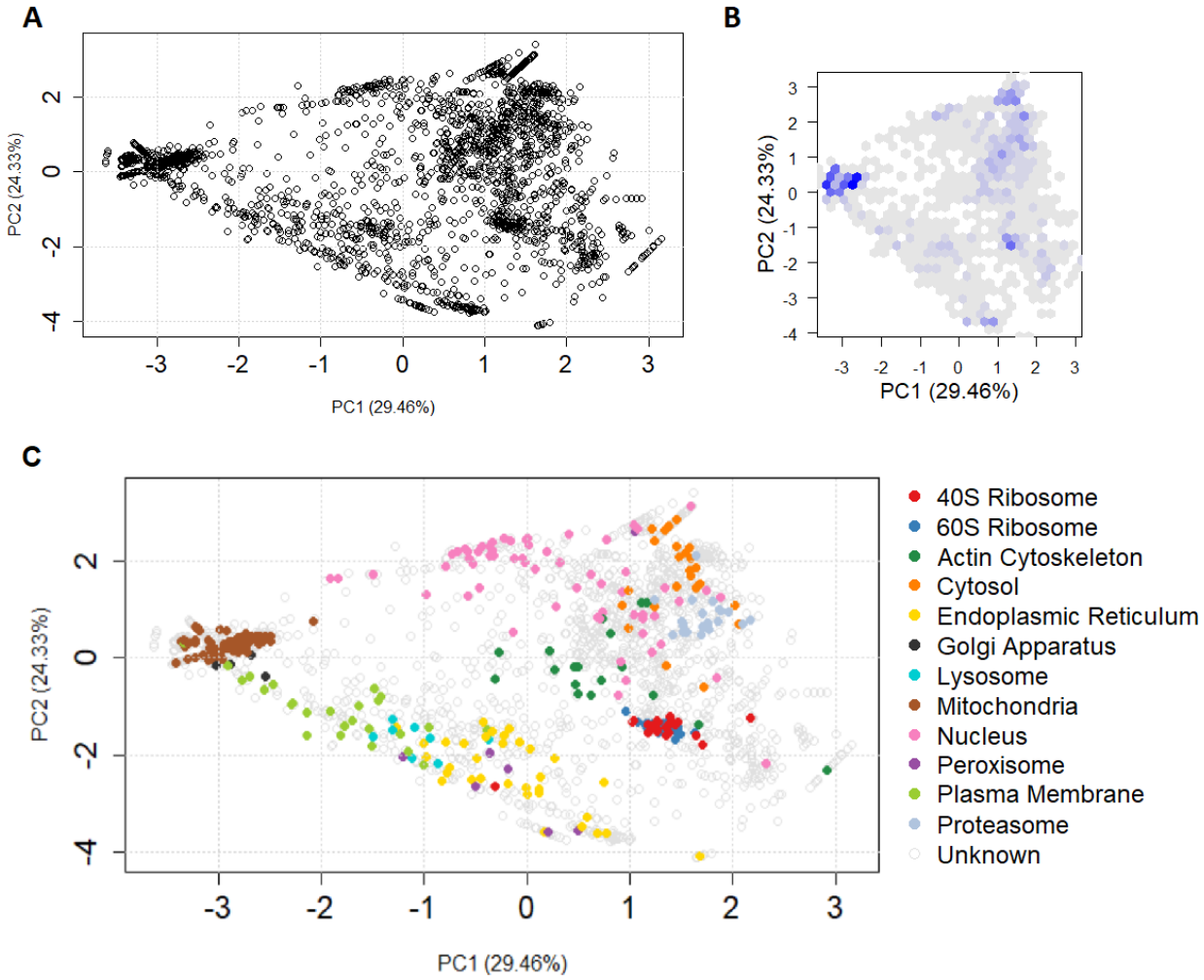

Figure 5. Protein clustering of differential centrifugation fractions. (A) Clustering of proteins quantified in the centrifugation fractions displayed in a PCA plot. (B) A hexbin plot showing the same principal components as in (A) shows regions of high protein density (blue) and low protein density (white), indicating clusters. (C) Organelle clustering is displayed by mapping protein markers to the PCA plot.

Marker occupancy profiles show distinct pelleting behavior of individual organelles (Fig. 6). Organelles like Golgi, lysosome and mitochondria have one well defined peak, each at a different fraction, where relative intensity is highest, after which relative intensity rapidly decreases. Other organelles have a

broader distribution of intensity over the fractions. It should be noted that some markers show missing values, these usually correspond to very low concentration. Taking this into account the profiles of each organelle appear as unique and could thus be used to train an organellar classification algorithm.

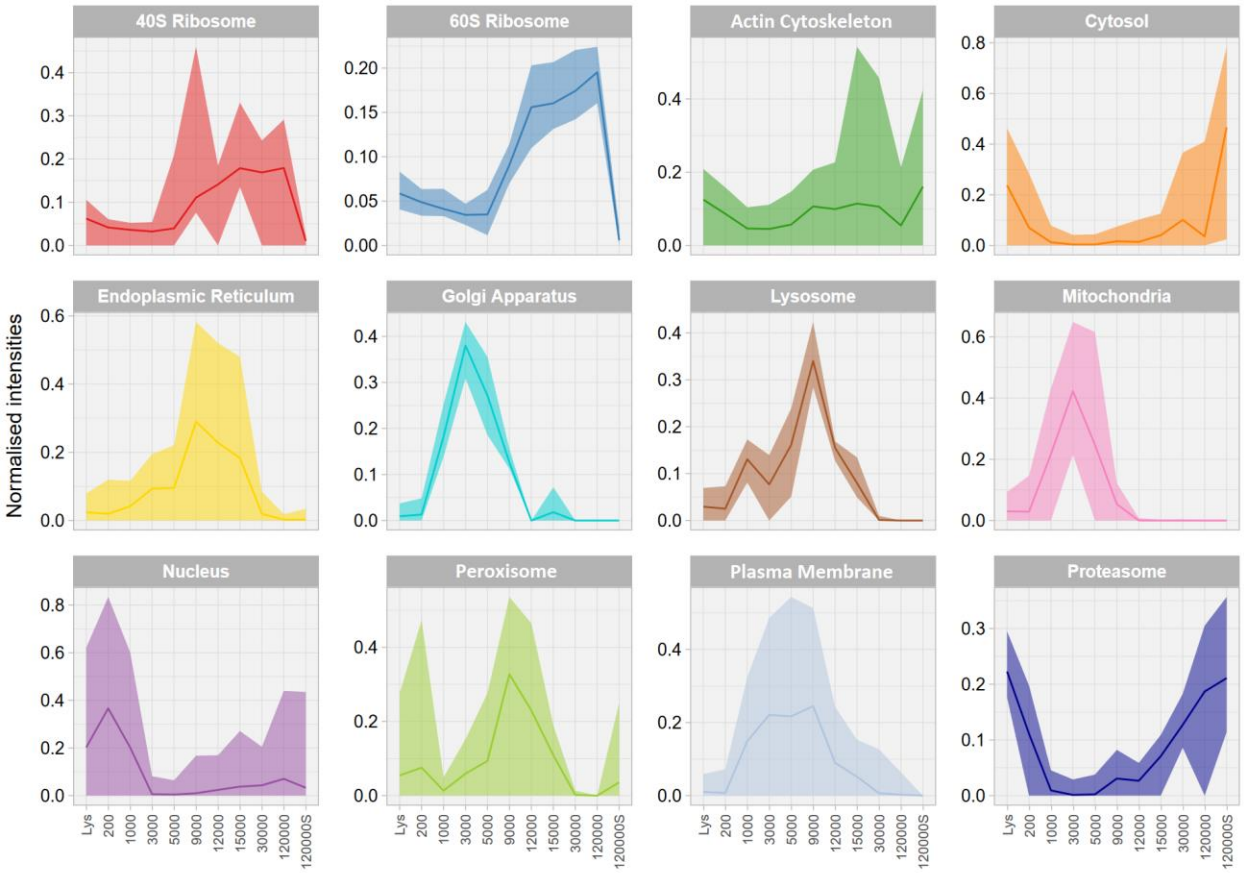

Figure 6. Organelle marker occupancy profiles. Human protein markers were applied to the dataset and the normalized intensities were mapped to show abundance distribution profiles. X-axis denotes the centrifugation speed (g) of the subcellular fractions starting from the lysate (Lys) to the 120.000g supernatant (S) fraction.

TMT-SILAC protein identification and quantification

In the final experiment SILAC light and heavy labeled cells were treated with 10 µm DMSO and PalmB, respectively, for 3h. After incubation the cells were harvested, counted and combined in a 1:1 ratio before lysis and fractionation using differential centrifugation. Compared to the LFQ experiment this resulted in the identification of fewer proteins with 2746 and 2138 proteins for DMSO and PalmB, respectively. However, these proteins contained far fewer missing values as only 155 and 183 proteins were filtered for DMSO and PalmB. Compared to the LFQ experiment, the SILAC-TMT translocation experiment resulted in less clustering. Most proteins localized to the center of the PCA plot (Fig 7C/D) with a minor side cluster on the right side of the plot. This lack of clustering may resolve itself once protein markers are annotated and the data is viewed from different principal components. Although reduced compared to the LFQ experiment, the clustering of the DMSO and PalmB datasets showed high similarity. This was expected, as most proteins were not predicted to translocate. This is promising as high similarity between treatment groups is required for the training of the classification algorithm.

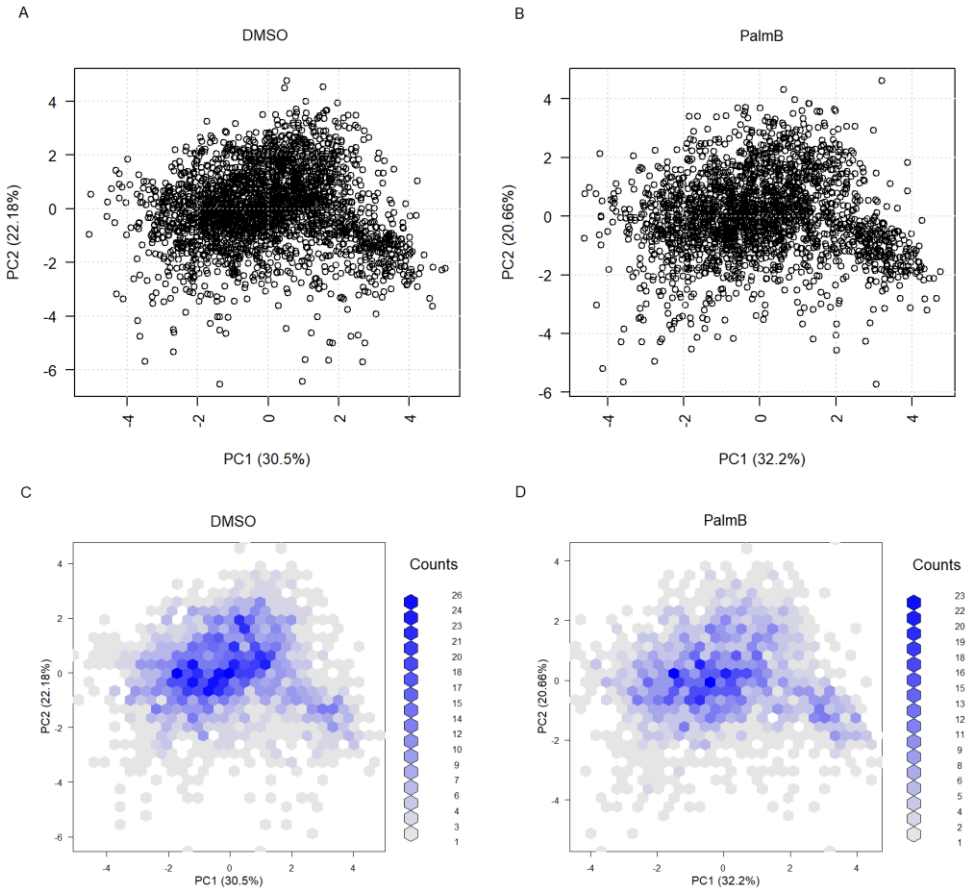

Figure 7. Clustering of proteins in DMSO and PalmB treated cells. Clustering of proteins identified in a spatial proteomics experiment for DMSO (A) and PalmB (B) treated cells. Hexbin plots showing cluster density for DMSO (C) and PalmB (D).

Channel intensity distribution

Relative TMT channel intensities were compared to identify channels with abnormally high or low yield. Lower quantitation intensities were recorded for channel 126, 127N, 130C and 131 in both DMSO and PalmB treated cells, even though equal amounts of peptide were labeled across all TMT channels (Fig. 8). The lower intensities are suboptimal as it could indicate biased protein profiles. Removal of the low intensity channels did equalize the intensities of the remaining channels, but did not improve clustering (Sup. Fig. 7). Additionally, the removal of these channels led to a large reduction of the dataset potentially complicating organelle classification and translocator identification. For these reasons it was decided to include all channels in the subsequent data analysis. Fortunately, the channel intensities were nearly identical between the treatment groups, albeit with PalmB displaying a slightly higher intensity across all fractions. This high similarity is likely a result of the SILAC labeling as it allowed the combination of cell cultures ensuring identical sample preparation.

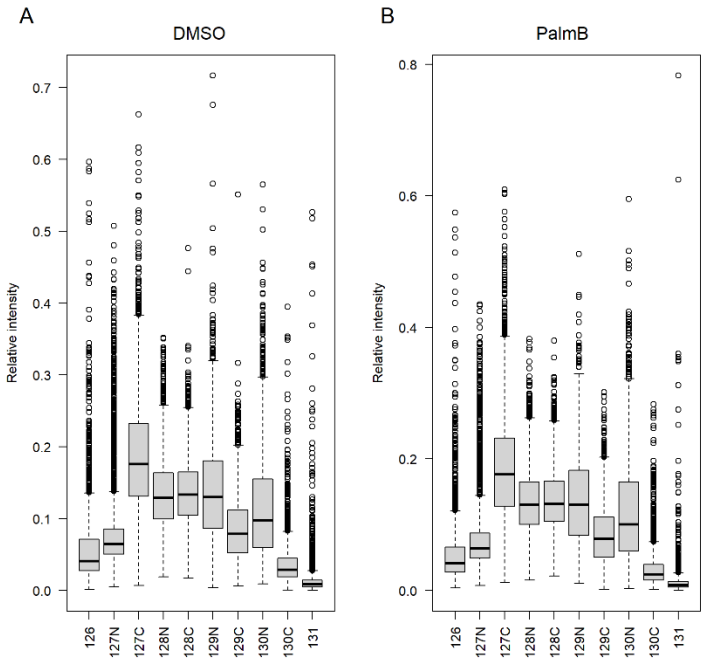

Figure 8. TMT channel intensity distribution. Relative quantitation intensities (y-axis) for individual TMT channels (x-axis) are displayed in boxplots for DMSO (A) and PalmB (B) treated cells.

Organelle clustering

Organelle prediction requires protein markers of known localization for training the classification algorithm. In order to determine organelle separation, protein markers present in the pRoloc package (v1.30.0) were applied to the dataset and visualized in a PCA plot. Mapping of these protein markers indicated that not all organelles separated in distinct clusters (Fig. 9). The mitochondria and nucleus separated in well defined clusters, but other organelles displayed high overlap. These overlapping organelles also did not separate when visualized in other principal components (Sup. Fig 8). For the Golgi, lysosomes and peroxisomes less than the minimal number of thirteen markers required for SVM prediction were mapped. Evidently, performing organelle prediction with this data was expected to result in low prediction scores.

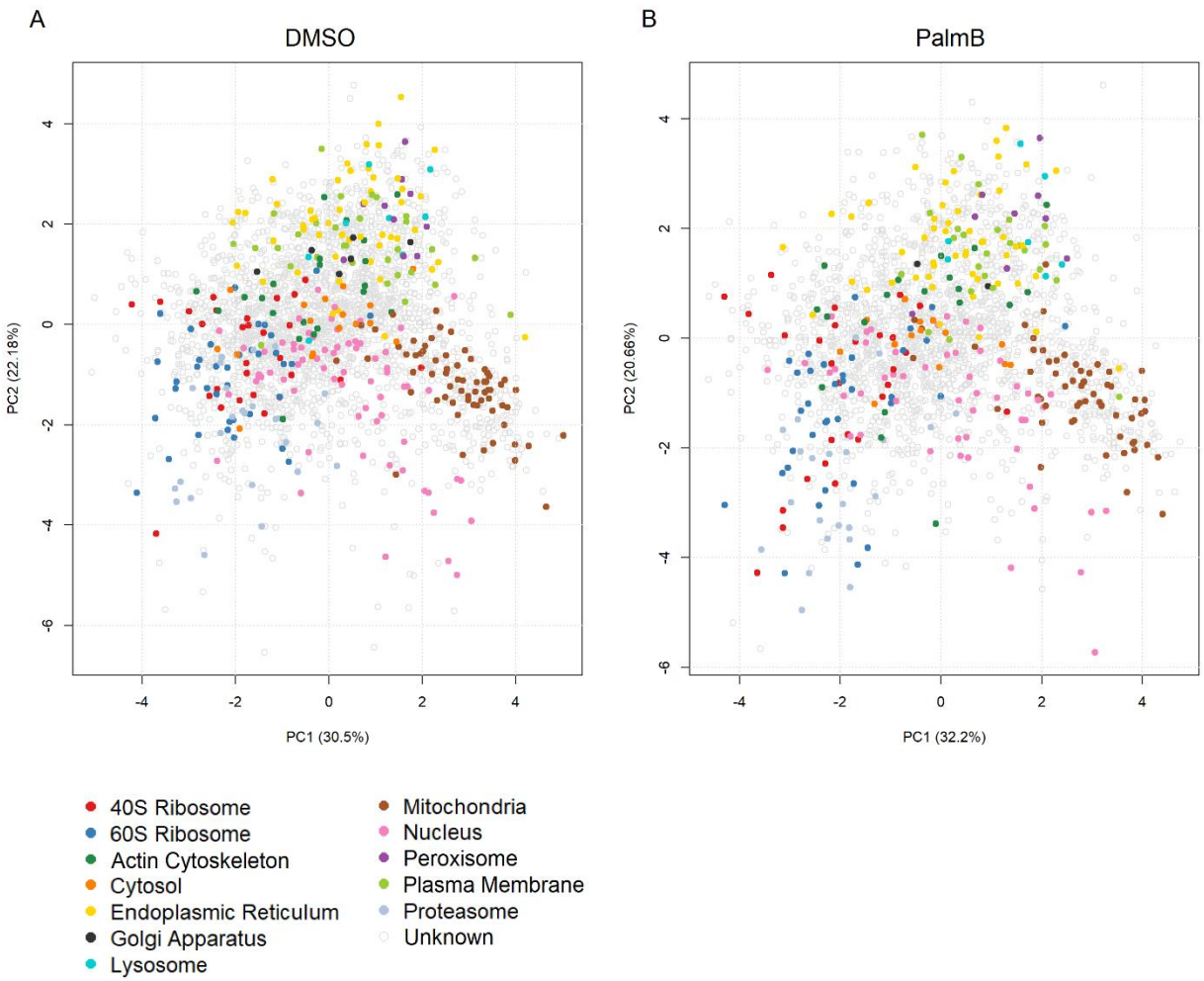

Figure 9. Organelle clustering of DMSO and PalmB treated cells. Protein markers were applied to a PCA plot of DMSO (Left) and PalmB (right) treated cells indicating organelle clustering.

Overlapping marker occupancy profiles

The lack of organelle clustering was investigated by examining organelle marker profiles. Several individual organelles exhibited similar marker profiles (Fig. 10) explaining the overlapping organelle clusters. To increase prediction accuracy, organelles with similar marker profiles were combined (Sup. Fig. 9). Nine organelles were combined resulting in four organellar classes: lysosome/peroxisome, cytosol/actin cytoskeleton, ribosome/proteasome and endoplasmic reticulum/plasma membrane (ER/PM). Organelles displaying well separated clustering, like the nucleus and mitochondria, were not combined. Less than five markers were mapped to the Golgi making it hard to combine with other organelles, for this reason they were set to unknown. Lastly, proteins markers which exhibited large changes in profiles between DMSO and PalmB were excluded from the training set.

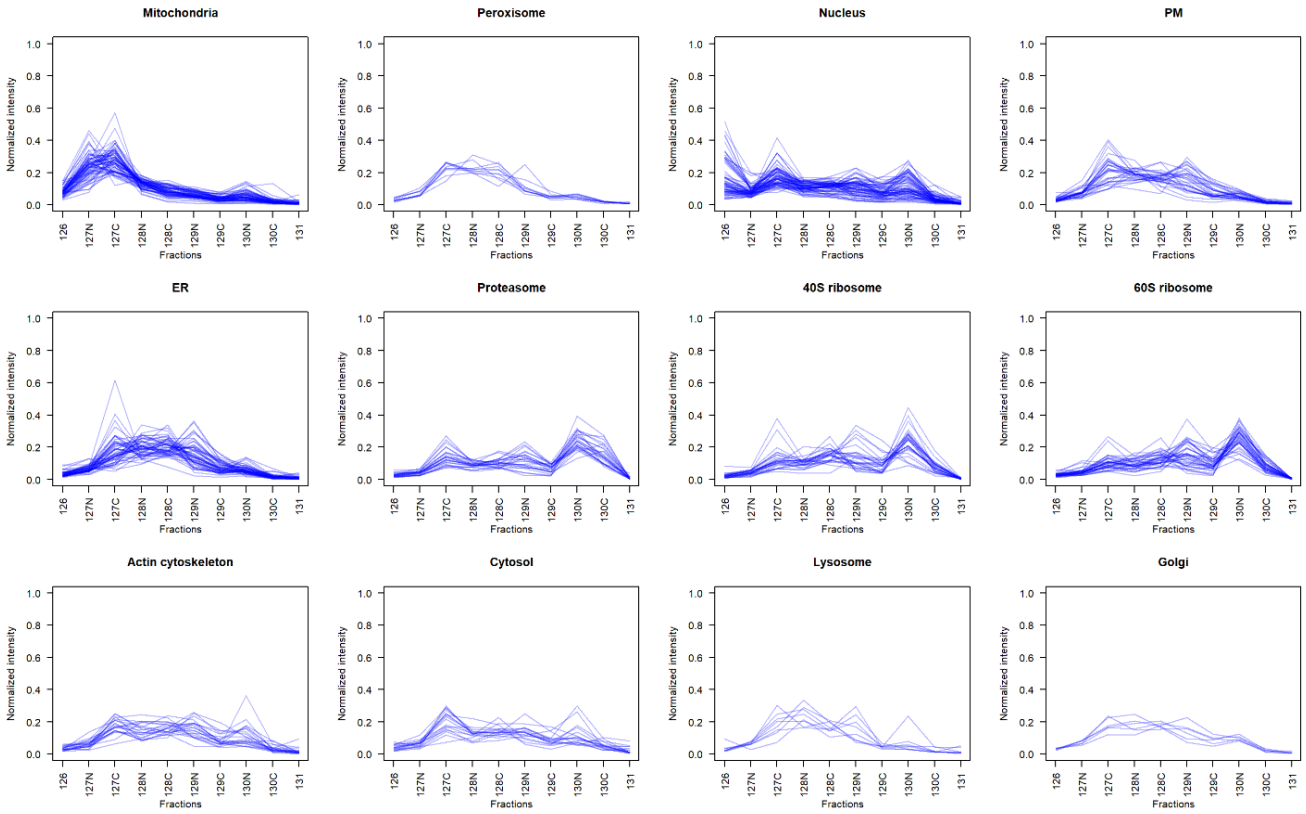

Figure 10. Organelle marker occupancy profiles of DMSO treated cells. Normalized intensity profiles of marker proteins are plotted for individual organelle classes for DMSO treated cells. The X-axis denotes the TMT labels used to label the differential centrifugation fractions.

Clustering of combined organelle classes.

Clustering was greatly improved by combining organelle classes, as less overlap was observed in the clustering of these classes (Fig 11). The ER/PM and ribosome/proteasome classes showed improved clustering compared to the individual organelle clustering. However, the lysosome/peroxisome still overlapped with the ER/PM. Additionally, the cytosol/actin cytoskeleton was present at the interface of all other organelle classes. Despite improved clustering, the organelle class separation is still suboptimal, hence the prediction scores for some organelle classes are predicted to be low.

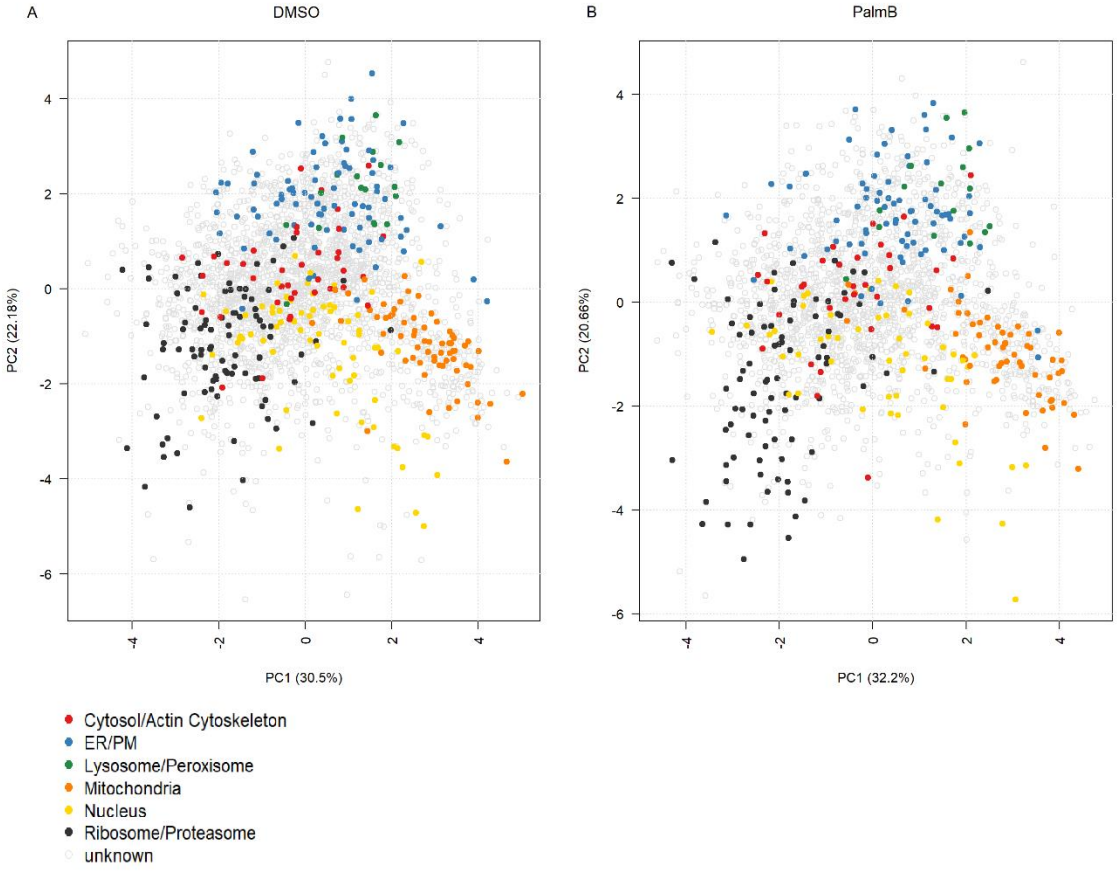

Figure 11. Clustering of combined organelle classes. Organelles with similar protein marker profiles were combined into organelle classes and the resulting marker classes were annotated on PCA plots of DMSO (A) and PalmB (B) treated cells.

Organelle classification

In order to increase resolution, the DMSO and PalmB datasets were combined for SVM training. This meant combining both datasets as two replicates into one MS proteomics dataset and filtering proteins not identified in both. The training results were applied to DMSO and PalmB separately in order to identify changes in organellar prediction. Proteins scoring below the median organelle specific prediction score were left unassigned (grey circles, Fig. 12A/B). In line with the organelle class clustering the prediction scores were relatively high for mitochondria and nucleus, intermediate for ER/PM and ribosome/proteasome, and low for cytosol/actin cytoskeleton (Fig. 12 C/D). While, lysosomal/peroxisomal proteins were assigned to the PalmB dataset with low prediction scores, no proteins were assigned to this class in the DMSO dataset. This is likely because the small number of markers in this class makes the predictions less reliable and thus less consistent among treatment groups.

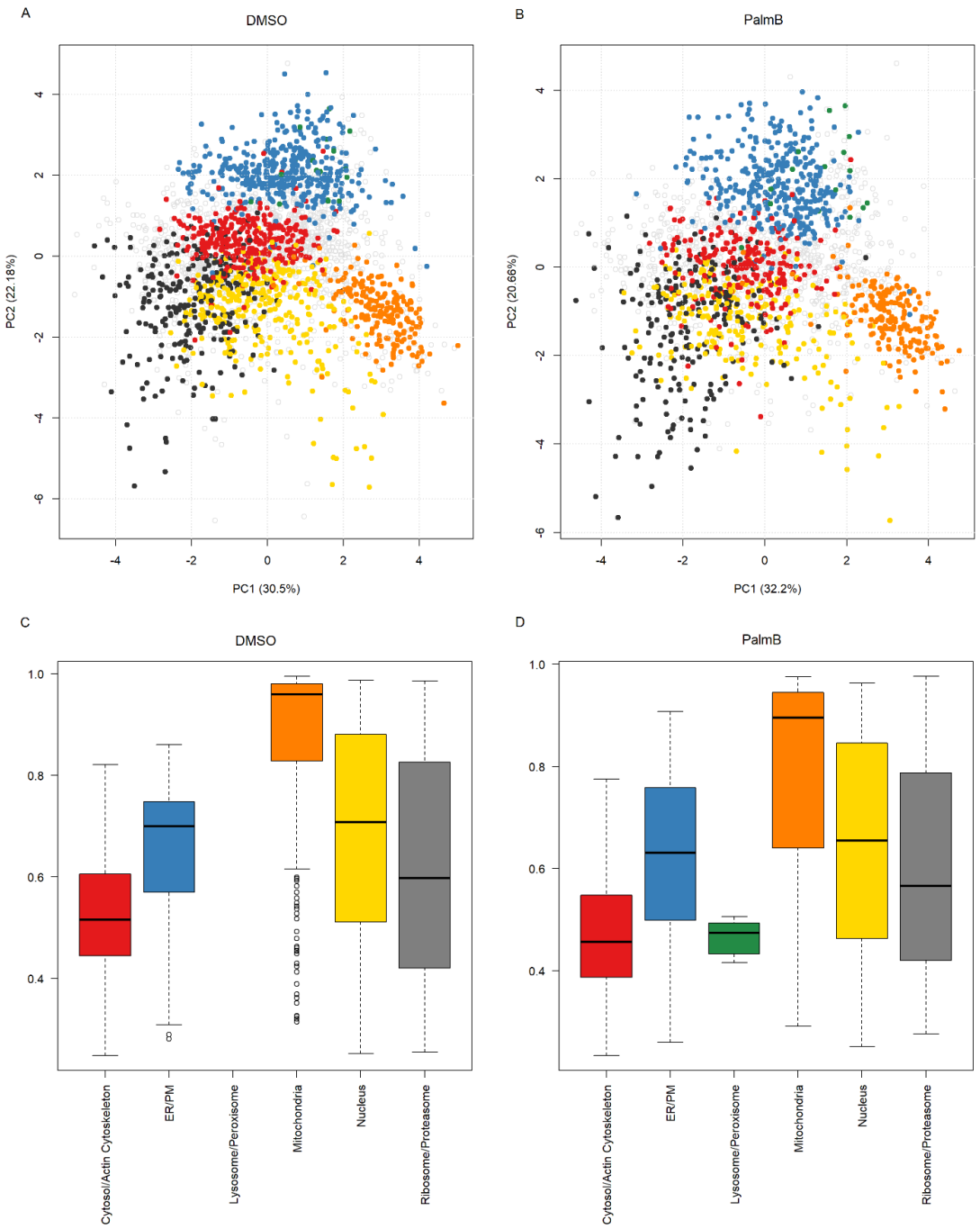

Figure 12. Organelle class prediction of DMSO (left) and PalmB (right) treated cells. Proteins were classified into subcellular niches based on combined classes of marker proteins (top). Proteins below the median organelle class specific prediction score were left unassigned (grey circles). Prediction scores of individual organelle classes are visualized in boxplots for DMSO (C) and PalmB (D) treated cells.

S-Palmitoylation enrichment in translocating proteins

Translocating proteins were identified by calculating magnitude of translocation scores (M scores). Delta profiles were generated by subtracting treated from untreated protein profiles. Outliers were detected by calculating the squared Mahalanobis distances followed by the adjusted P value. Adjusted P values were converted to Q values by multiplying by protein rank (from low to high adjusted P value) and dividing by the total number of proteins. Finally the M scores were calculated by taking the common logarithm of the Q values. Using this method we identified 132 proteins with an M score above 0 among 1847 proteins common between DMSO and PalmB treated cells. A minimum of 3 identified peptides was set as a threshold to eliminate poorly characterized proteins. After applying this threshold, 48 putative S-palmitoylation dependent translocating proteins remained. A Swisspalm database search found a large portion of these translocators to be present in S-palmitoyl-proteome studies (68.8%) compared to the full proteome (18.1%) (Sup. Fig 13). Furthermore, in-house unpublished metabolic labeling (MLCC) and acyl biotin exchange (ABE) studies of HEK293T and SH-SY5Y cells identified 70.8% of these translocators. Of the 48 translocators the only proteins not identified in S-palmitoylation enrichment studies include C19orf25, CDV3, EEF1AKNMT, ELP1, HELZ, PFDN1, TMSB10 and WASHC2C. The enrichment of S-palmitoylated proteins among the PalmB mediated translocators may indicate a role for S-palmitoylation in the localization of these enriched proteins.

Membrane association of translocating proteins

In order to establish whether transmembrane proteins translocate as frequently as peripheral membrane or cytosolic proteins a database search was performed on the 48 translocating proteins. The Swisspalm database identified 40% as cytosolic and 17% as transmembrane proteins among the translocators (supplemental figure 14). This would indeed imply that cytosolic proteins translocate more frequently than transmembrane proteins. However, Swisspalm identified 44% of proteins as ‘other’. A Uniprot database search of these proteins revealed that the membrane association and/or subcellular localization of these proteins was not annotated or ambiguous. Given the undetermined association of a large fraction of the translocating proteins it is impossible to draw any conclusions on translocations for different types of membrane proteins.

Translocation patterns

Different types of intracellular translocations were observed based on their predictions. BYSL was shown to completely translocate from the ribosome/proteasome to the mitochondria with high prediction scores of 0.80 and 0.84 respectively. 33% of proteins were shown to partially translocate within their organelle class. These intra-organellar translocations were attributed to mitochondrial (6), ribosomal/proteasomal (4), nucleus (5), and cytosolic/actin cytoskeleton (1) proteins. Five partial extra-organellar translocations were observed wherein a protein moved from one compartment with a high score (>0.80) to another with a low score (<0.80), or vice versa. Lastly, 26 partial inter-organellar translocations were observed. These translocations were characterized by different organelle predictions for DMSO and PalmB, of which both associated with low prediction scores. A list of translocators and their types of translocation can be found in table I.

Table I. Changes in organellar class predictions for translocating proteins

Gene names	M scores	Swisspalm	Prediction DMSO	Prediction score DMSO	Prediction PalmB	Prediction score PalmB	Translocation Type
ADRM1	2,3	+	Ribosome/ Proteasome	85%	Ribosome/ Proteasome	77%	intra
ALDH3A2	4,2	+	Cytosol/Actin Cytoskeleton	46%	ER/PM	45%	inter
ALDH7A1	2,8	+	Mitochondria	73%	Ribosome/ Proteasome	30%	inter
ATAD3B	5,7	+	Mitochondria	95%	Mitochondria	93%	intra
ATP5MF	12,4	+	Mitochondria	35%	Mitochondria	90%	intra
BCLAF1	5,5	+	Nucleus	95%	Nucleus	63%	intra
BYSL	4	+	Ribosome/ Proteasome	80%	Mitochondria	84%	complete
BZW2	17,5	+	Ribosome/ Proteasome	74%	Cytosol/Actin Cytoskeleton	63%	inter
C19orf25	23,6	-	Ribosome/ Proteasome	28%	ER/PM	86%	extra
CDV3	23,2	-	Ribosome/ Proteasome	29%	Cytosol/Actin Cytoskeleton	50%	inter
COPS8	2,7	-	Nucleus	43%	Cytosol/Actin Cytoskeleton	71%	inter
CREB1	4,8	-	Nucleus	85%	Nucleus	94%	intra
DNAJB11	7,6	-	ER/PM	75%	Nucleus	56%	inter
ECHS1	10,9	+	Cytosol/Actin Cytoskeleton	25%	Mitochondria	79%	inter
EEF1AKNMT	29,8	-	Cytosol/Actin Cytoskeleton	58%	Ribosome/ Proteasome	30%	inter
EIF2S1	2,9	+	Ribosome/ Proteasome	88%	Ribosome/ Proteasome	39%	intra
ELP1	12,8	-	Ribosome/ Proteasome	31%	Cytosol/Actin Cytoskeleton	32%	inter
ERH	7,4	+	Ribosome/ Proteasome	55%	Nucleus	68%	inter
GCDH	2,3	-	Mitochondria	97%	Mitochondria	95%	intra
GFM1	5	-	Mitochondria	99%	Mitochondria	68%	intra
GSTP1	4,6	+	Cytosol/Actin Cytoskeleton	37%	Cytosol/Actin Cytoskeleton	29%	intra
H2AX	2,6	+	Nucleus	41%	Nucleus	47%	intra
HELZ	5,4	-	Nucleus	48%	Cytosol/Actin Cytoskeleton	54%	inter
HMGB2	5,7	+	Nucleus	27%	Nucleus	57%	intra
HMGN1	7,9	+	Nucleus	74%	Nucleus	83%	intra
HSPA14	6,7	+	Nucleus	98%	Cytosol/Actin Cytoskeleton	57%	extra

Gene name	M score	Swisspalm	Prediction DMSO	Prediction score DMSO	Prediction PalmB	Prediction score PalmB	Translocation Type
IDH3A	5,6	+	Mitochondria	99%	Ribosome/ Proteasome	58%	extra
MCM6	2,6	+	Cytosol/Actin Cytoskeleton	42%	Ribosome/ Proteasome	52%	inter
NDC1	64,3	+	Ribosome/ Proteasome	29%	Mitochondria	89%	extra
NOC3L	2,5	+	ER/PM	52%	Nucleus	57%	inter
OFD1	3,1	+	Ribosome/ Proteasome	30%	Cytosol/Actin Cytoskeleton	75%	inter
OSBPL8	23,4	+	ER/PM	65%	Ribosome/ Proteasome	64%	inter
PBXIP1	13,2	+	ER/PM	74%	Mitochondria	93%	extra
PFDN1	23,2	-	Cytosol/Actin Cytoskeleton	40%	Ribosome/ Proteasome	30%	inter
PFN1	10,9	+	Cytosol/Actin Cytoskeleton	69%	Ribosome/ Proteasome	38%	inter
PGAM1	29,7	+	Ribosome/ Proteasome	39%	Cytosol/Actin Cytoskeleton	48%	inter
PSMD7	6,2	-	Ribosome/ Proteasome	66%	Ribosome/ Proteasome	95%	intra
PTMA	66,5	+	Ribosome/ Proteasome	29%	Cytosol/Actin Cytoskeleton	45%	inter
PTMS	6,6	+	Ribosome/ Proteasome	29%	Ribosome/ Proteasome	30%	inter
RBM27	18,2	-	Ribosome/ Proteasome	29%	Cytosol/Actin Cytoskeleton	43%	inter
SLC25A5	16,5	+	Mitochondria	81%	Mitochondria	92%	intra
SLC25A6	18,5	+	Ribosome/ Proteasome	29%	Mitochondria	76%	inter
SUGT1	5,9	+	Cytosol/Actin Cytoskeleton	68%	Ribosome/ Proteasome	30%	inter
TFAM	4,7	+	Mitochondria	77%	Mitochondria	92%	intra
TMED9	14,5	+	Ribosome/ Proteasome	75%	Ribosome/ Proteasome	35%	inter
TMSB10	23,1	-	Ribosome/ Proteasome	29%	Ribosome/ Proteasome	30%	intra
TUBB	2,3	+	Cytosol/Actin Cytoskeleton	47%	Ribosome/ Proteasome	36%	inter
WASHC2C	32,5	-	Ribosome/ Proteasome	29%	Mitochondria	54%	inter

Gene names of translocating proteins with their M scores and their presence (+) or absence (-) in palmitoyl-proteomes in the Swisspalm database. Changes in prediction and prediction scores are displayed for DMSO and PalmB. Different types of translocations were observed based on predictions.

Interactions among translocators

To gain further insight into the nature of the translocating proteins a protein-protein interaction network search was performed using the STRING-db database. This indicated that a considerable number of translocators interact with each other (Fig. 13). The high number of interactions may indicate that some translocations may not be caused by altered S-palmitoylation, but rather by the translocation of a binding partner. Six clusters of interacting proteins were found to have similar changes in organelle class prediction, albeit with different prediction scores among interacting proteins. However, similar changes in organelle class predictions for interacting partners does not automatically translate to identical changes in protein profiles. Hence, comparison of organelle predictions is not a reliable method to establish protein complex translocations. In order to determine whether interacting proteins co-translocate the DMSO and PalmB profiles of these interacting proteins were compared.

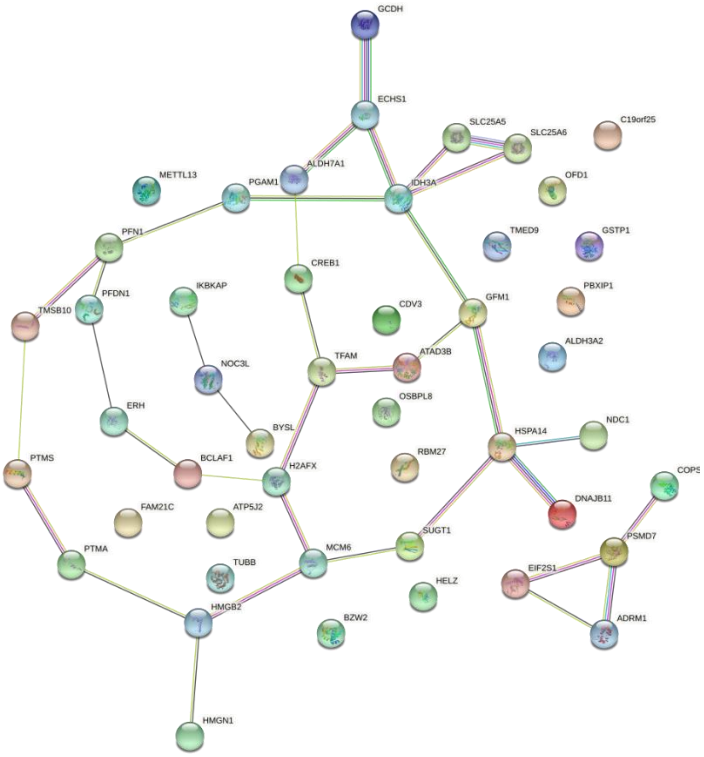

Figure 13. Protein interaction network of translocating proteins. Translocators were searched in the string-db protein interaction database. 36 links were found for 48 nodes. The average node degree was 1.5. Significant clustering is observed as the PPI enrichment p-value is 0.000399.

Most interacting proteins did not display similarities in their protein distribution profiles. Furthermore, some interacting partners, like IDH3A and ECHS1, exhibited opposite changes in protein distribution profiles (Fig. 14). For these proteins the DMSO profile of IDH3A matched the PalmB profile of ECHS1 and vice versa. Similarly TFAM and GFM1 which share ATAD3B as interacting partner also showed opposite protein distribution profiles. This would indicate that under the same treatment conditions IDH3A & ECHS1, and TFAM & GFM1 would not be present at the same intracellular localization to allow for interaction. This would suggest these proteins in DMSO and PalmB treated HEK293T cells do not interact at all.

Two binding partners that likely co-translocated were TMSB10 and PTMS. These proteins had strikingly similar profiles in both DMSO and PalmB treated cells. The high profile similarity in both TMSB10 and PTMS may imply that these proteins translocate as a complex. If the translocation occurs through a change in S-palmitoylation state it may be that S-palmitoylation of only one binding partner is enough to translocate both proteins. On the contrary, PTMA, an interactor of PTMS, had a similar DMSO profile, which would allow for protein interaction, but a different PalmB profile. This could indicate that PTMA translocated independently of PTMS and TMSB10.

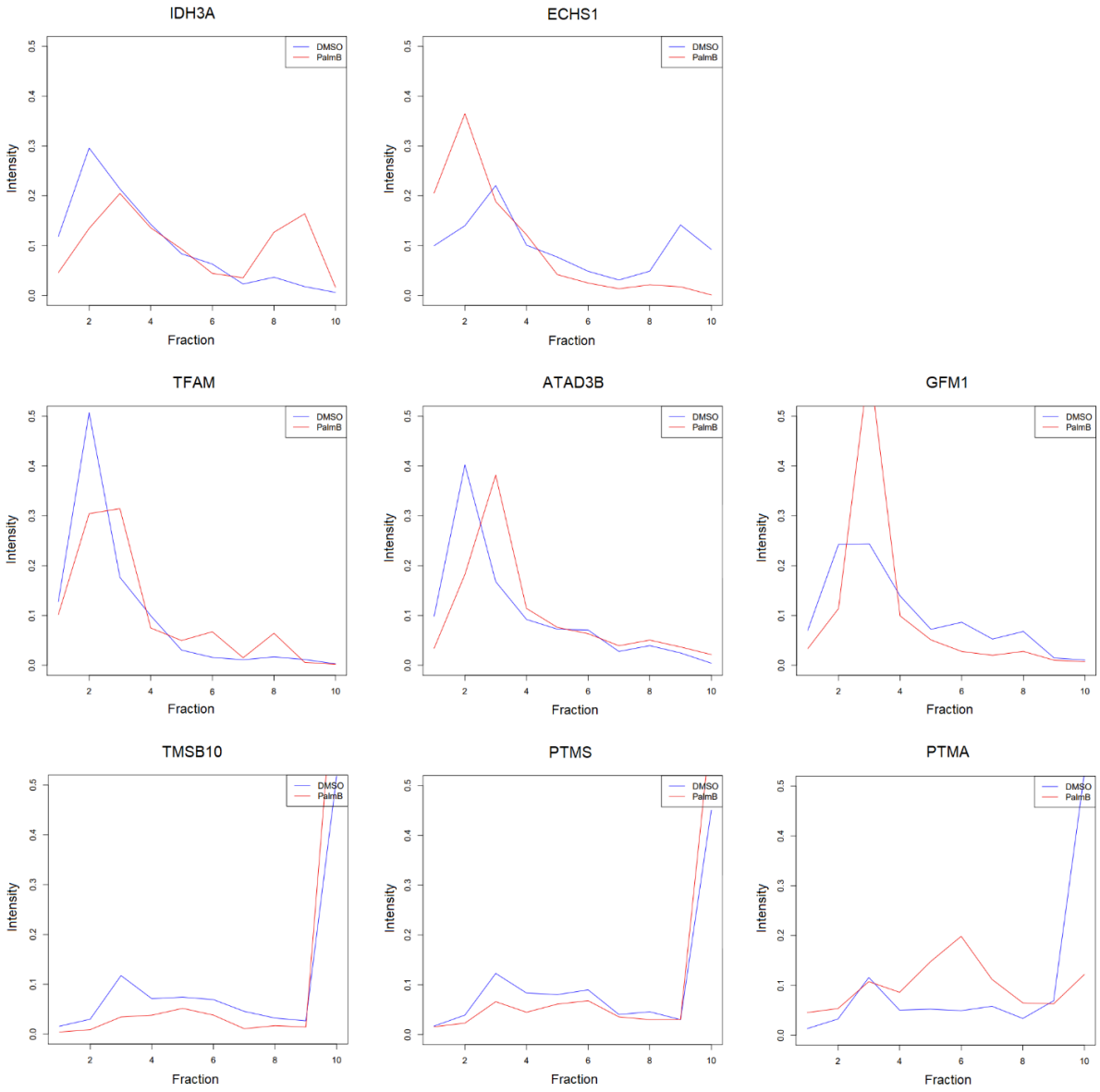

Figure 14. Normalized intensity profiles of potentially interacting and translocating proteins. Top: ECHS1 and IDH3A. Middle: TFAM, ATAD3B and GFM1. Bottom: TMSB10, PTMS and PTMA. The Y-axis denotes the normalized intensity of the protein profiles of DMSO (blue) and PalmB (red) treated cells, the x-axis denotes the fractions (1-10).

Discussion

Inhibition of APT1 and APT2 by PalmB

PalmB exhibited a four-fold stronger inhibition for APT2 compared to APT1 in HEK293T lysates. While initial studies focused solely on characterizing APT1 inhibition[36], later studies determined the IC_{50} of PalmB for APT1 and APT2 to be very similar[47]. These studies however, utilized recombinantly expressed and purified proteins making comparisons with activity assays in lysates difficult. Interestingly, *in situ* ABPPs demonstrated an even stronger difference in inhibition for APT1 and APT2. This may be the result of a difference in accessibility. While both APT1 and APT2 have been found to be present in the cytosol[48,49], there is evidence to suggest that APT1 may also reside in the mitochondria[50]. While PalmB is known to be cell-permeable and capable of reaching the mitochondria, the extent of membrane-permeability and accessibility to the mitochondria is unknown. As a result, PalmB may require higher concentrations to enter the mitochondria explaining the weaker inhibition of APT1 in live cells.

The cause and effect of uneven TMT channel intensities

Combined SILAC-TMT labeling was used to sample pooling in the translocation experiment. Despite the care taken to ensure digestion and TMT labeling of equal amounts of protein, the relative TMT intensity was unequal for the TMT channels. TMT labeling efficiency was determined to be above 95% and any variations in labeling and peptide quantitation did not reflect the relative intensity distribution seen for the translocation experiment. Instead, the differences in channel intensities may have been caused by human error during sample pooling, or more likely by the MS method used for peptide quantitation or the subsequent data processing. For the translocation experiment a standard TMT10-plex method was used to identify peptides in MS1 and quantify TMT reporter ions in MS2. In contrast, SILAC-TMT labeled samples are more commonly analyzed by MS3 based methods with synchronous precursor selection[52–55]. We opted for MS2 as it has higher sequencing speed compared to MS3. However, MS2 suffers from ratio distortion caused by co-isolating ions which may have played a part in the uneven TMT channel intensities.

As mentioned, the data processing method employed may have also caused the uneven TMT channel intensities. A dual search strategy was performed in Proteome Discoverer by both doing a SILAC light and heavy search with TMT on lysine as fixed and TMT on N-termini as variable modifications[52]. This strategy may affect FDR levels as it may force heavy labeled peptides to be wrongfully identified in the light search and vice versa. Alternatively, a single search with TMT labels as static and SILAC amino acids as dynamic modifications could have been performed[53,55]. While the single search strategy was our preferred method, it resulted in very high mass error when applied in MaxQuant. A comparison of data processing methods for the generated SILAC-TMT data could be useful as there is no consensus in literature regarding the best method.

The uneven TMT channel intensities resulted in low relative intensities of channel 126, 127N, 130C and 131 indicating that the quantitation values of these channels were low for all quantified proteins. This was reflected in the organelle marker profiles, which were discernible only by intensity differences in the other channels. This information loss made some organelles indistinguishable leading to the observed overlapping clusters. In contrast the LFQ experiment displayed mostly even relative intensities

for the centrifugation fractions. Not only did the organelle marker profiles appear different in the LFQ experiment, they were also more discernable resulting in more pronounced clustering.

Organelle prediction threshold

Organelles with similar protein marker profiles were combined to increase prediction scores. This resulted in varying prediction scores across organelle classes. Different methods for setting a threshold could have been used for keeping low scoring proteins unassigned. A universal threshold could have been set, but due to the varying organelle scores observed this would have reduced the protein assignment, or it would have required lowering the threshold. A threshold could also have been set based on reproducibility, by requiring two out of three replicates to have the same classification[57]. However, we did not have multiple replicates. Alternatively, a threshold could be set at a 5% FDR by comparison of predictions with a database[41]. In the end, the threshold was set at the median organelle prediction score resulting in organelle specific thresholds.

Characterization of translocating proteins

Despite large differences in TMT channel intensity, translocating proteins could still be identified by comparison of DMSO and PalmB protein profiles. While it is also possible to determine translocations based on prediction changes[58], this qualitative method is only suitable when prediction accuracy is high. Additionally the translocations need to be large enough to result in a change of assignment, which for most translocating proteins may not be the case. Another method to identify translocating proteins is TRANSPIRE[59], which employs a probabilistic Gaussian process classifier. However, this classifier is trained with semisynthetic data of altered organelle marker profiles which may not represent the translocations observed in a cellular context.

Using a quantitative method we identified 48 proteins to be potentially translocated in response to PalmB treatment. We found an overrepresentation of S-palmitoylated proteins among these translocators. It could be that these identified translocators are associated to cellular compartments known for their dynamic localization, like transport vesicles and endosomes. However, this would not explain the overrepresentation of S-palmitoylated proteins, as non-palmitoylated endosomal and vesicular proteins would then also be identified as translocating. More likely, the S-palmitoylated translocators identified may change localization in response to PalmB mediated changes in their S-palmitoylation stoichiometry.

Inhibition of depalmitoylases by PalmB does not lead to an absolute change in protein S-palmitoylation state, rather it changes the stoichiometry of S-palmitoylated proteins. As a result partial translocations are observed more often than complete translocations. This is exemplified by BYSL, which was the only protein shown to change compartments with high confidence scores. Of the partial translocations observed, one third was intra-organellar. For these translocations a protein was assigned to the same organelle, albeit with different prediction scores. This can be attributed to a movement within an organelle, or a changed distribution between two organelles wherein the largest portion is still associated with one organelle. However, these two types of movement cannot be distinguished with this data. Another translocation type observed was the extra-organellar translocation, in which organelle assignments changed associated with a change from a high to low prediction score, or vice versa. These patterns may correspond to proteins that predominantly locate to one organelle, while also having a small portion that locate to another organelle. Inhibition by PalmB may shift this distribution leading to a different assignment with a lower score. Comparison of PCA plots is the most reliable

method to evaluate the direction of these translocations. The majority of translocations exhibited a change in assignment associated with low prediction scores indicative of inter-organellar translocations. These low scores indicate that these proteins have a broad organelle distribution. Treatment with PalmB changes this distribution, but not enough to result in a single organelle association for the protein.

Potential interaction among translocators

A database search identified a high degree of interaction among the potential translocators. This could imply that some translocations may occur in response to the translocation of a binding partner, rather than in direct response to PalmB. However, many of these identified protein interactions have not been established in biochemical assays, but in co-expression assays. This would explain why the DMSO profiles of the majority of these linked proteins do not match, as proteins that are physically associated would show identical centrifugation profiles. In fact, centrifugation based fractionation methods have been successfully used to identify protein-protein interactions[60]. Potential Interacting proteins that did share changes in profiles suggesting co-translocation are TMSB10 and PTMS. So far the only established link between these proteins is the increased expression in breast cancer cells and tissues[64]. PTMA, which has been validated to interact with PTMS[68,69], shares a similar DMSO profile with PTMS and TMSB10. The PalmB profile of PTMA is however, distinct from PTMS and TMSB10, indicating independent movement. While the high network connectivity between the translocators remains interesting, the effect of these supposed interactions on protein translocation remains to be explored.

Altered metabolism by PalmB

In vitro gel-based ABPPs, in contrast to in situ ABPPs, identified several proteins, aside from APT1 and APT2, to be inhibited by PalmB. While we were unable to characterize the inhibition of these enzymes, studies show PalmB to inhibit (in COS-7 cells) several serine hydrolases including ABHD6, ABHD4, ABHD16A, ABHD17A-C, PAFAH2 and several lipid metabolic enzymes like ACOT1, ACOT2, FASN, PNPLA6[51]. Although the PalmB concentration was minimized for the experiments, the possibility of inhibition of metabolic enzymes cannot be excluded. As such any potential translocating protein must be assessed critically. Among the 48 identified potentially translocating proteins were six metabolic enzymes. Two of these enzymes, PGAM1 and IDH3A, are not directly involved in fatty acid or lipid metabolism, but with glycolysis and the TCA cycle, respectively. In contrast ALD7A1, OSBPL8, ALDH3A2 and ECHS1 are involved in phospholipid, or fatty acid metabolism. Their enzyme activity and/or localization may have been altered by changes in cellular metabolism caused by PalmB rather than a change in S-palmitoylation.

Outlook

This study aimed to identify translocating proteins in response to the broad spectrum depalmitoylase inhibitor PalmB. While the spatial proteomics method has been demonstrated to be effective in separating organelles, the SILAC-TMT hyperplex method for quantification still requires optimization. Further research is necessary to evaluate the most suitable data processing method in regards to quantitation accuracy, mass error and FDR. Regardless, we were able to identify 48 potentially translocating proteins in response to PalmB treatment. The overrepresentation of S-palmitoylated proteins among these proteins suggests a link between their S-palmitoylation state and cellular localization. However, these translocating proteins as well as their link to S-palmitoylation still need to be validated. This is necessary as future research into the role of S-palmitoylation in intracellular protein localization may uncover fundamental processes involved in many debilitating diseases.

Acknowledgements

First and foremost, I would like to thank my supervisor Marc Baggelaar for his support and guidance during this project. His enduring optimism helped me see the silver linings in many of my failed or otherwise imperfect experiments. I would also like to thank Kelly Stecker for helping me prepare my SILAC experiment and helping me sort through all the different types of SILAC amino acids and TMT labeling kits. I am grateful for Mirjam Damen for fractionating my samples and Harm Post for advising me on my measurement method for my final experiment. Lastly I would like to thank Samiksha Sardana who was always around for quick advice, moral support or a chat and who helped me perform my 12 hour experiment.

References

1. Ko P, Dixon SJ. Protein palmitoylation and cancer. *EMBO Rep*. 2018;19(10). doi:10.15252/EMBR.201846666

2. Zaręba-Kozioł M, Figiel I, Bartkowiak-Kaczmarek A, Włodarczyk J. Insights Into Protein S-Palmitoylation in Synaptic Plasticity and Neurological Disorders: Potential and Limitations of Methods for Detection and Analysis. *Front Mol Neurosci*. 2018;11:175. doi:10.3389/FNMOL.2018.00175

3. Fukata Y, Iwanaga T, Fukata M. Systematic screening for palmitoyl transferase activity of the DHHC protein family in mammalian cells. *Methods*. 2006;40(2):177-182. doi:10.1016/J.YMETH.2006.05.015

4. Won SJ, Kit MCS, Martin BR. Protein depalmitoylases. *Crit Rev Biochem Mol Biol*. 2018;53(1):83. doi:10.1080/10409238.2017.1409191

5. B C, M P. G-protein-coupled receptors, cholesterol and palmitoylation: facts about fats. *J Mol Endocrinol*. 2009;42(5):371-379. doi:10.1677/JME-08-0114

6. E L, ED S, R H, et al. The effect of palmitoylation on the conformation and physical stability of a model peptide hormone. *Int J Pharm*. 2014;472(1-2):156-164. doi:10.1016/J.IJPHARM.2014.06.008

7. J V-T, H P. Swf1-dependent palmitoylation of the SNARE Tlg1 prevents its ubiquitination and degradation. *EMBO J*. 2005;24(14):2524-2532. doi:10.1038/SJ.EMBOJ.7600724

8. Perrody E, Abrami L, Feldman M, Kunz B, Urbé S, Goot FG van der. Ubiquitin-dependent folding of the Wnt signaling coreceptor LRP6. *Elife*. 2016;5(OCTOBER2016). doi:10.7554/ELIFE.19083

9. AE M, DE R, DJ S, et al. Reciprocal Phosphorylation and Palmitoylation Control Dopamine Transporter Kinetics. *J Biol Chem*. 2015;290(48):29095-29105. doi:10.1074/JBC.M115.667055

10. Blaskovic S, Blanc M, Goot FG van der. What does S-palmitoylation do to membrane proteins? *FEBS J*. 2013;280(12):2766-2774. doi:10.1111/FEBS.12263

11. O R, A P, M K, et al. An acylation cycle regulates localization and activity of palmitoylated Ras isoforms. *Science*. 2005;307(5716):1746-1752. doi:10.1126/SCIENCE.1105654

12. N Y, Y F, A S, T M, K K, M F. Identification of PSD-95 Depalmitoylating Enzymes. *J Neurosci*. 2016;36(24):6431-6444. doi:10.1523/JNEUROSCI.0419-16.2016

13. J R, JT K, SJ M. Palmitoylation regulates the clustering and cell surface stability of GABAA receptors. *Mol Cell Neurosci*. 2004;26(2):251-257. doi:10.1016/J.MCN.2004.01.012

14. DM Z, SW H, G C, HC H, CE M. Differential regulation of two palmitoylation sites in the cytoplasmic tail of the beta1-adrenergic receptor. *J Biol Chem*. 2011;286(21):19014-19023. doi:10.1074/JBC.M110.189977

15. AM E, SA S, O Z, et al. S-Palmitoylation Sorts Membrane Cargo for Anterograde Transport in the Golgi. *Dev Cell*. 2018;47(4):479-493.e7. doi:10.1016/J.DEVCEL.2018.10.024

16. C G, F M. Lipid rafts and raft-mediated supramolecular entities in the regulation of CD95 death receptor apoptotic signaling. *Apoptosis*. 2015;20(5):584-606. doi:10.1007/S10495-015-1104-6

17. K K, OV M, J F, A C. Flotillins: At the Intersection of Protein S- Palmitoylation and Lipid-Mediated Signaling. *Int J Mol Sci*. 2020;21(7). doi:10.3390/IJMS21072283

18. S O, TM S, A T, et al. Palmitoylation of cysteine 415 of CB 1 receptor affects ligand-stimulated internalization and selective interaction with membrane cholesterol and caveolin 1. *Biochim Biophys acta Mol cell Biol lipids*. 2017;1862(5):523-532. doi:10.1016/J.BBALIP.2017.02.004

19. E C, R S, R B, M V. The voltage-gated sodium channel β2 subunit associates with lipid rafts by S-palmitoylation. *J Cell Sci*. 2021;134(6). doi:10.1242/JCS.252189

20. X X, CF L, W L, et al. Acid Sphingomyelinase regulates the localization and trafficking of palmitoylated proteins. *Biol Open*. 2019;8(10). doi:10.1242/BIO.040311

21. R B, C B, DM K. Palmitoylation of amyloid precursor protein regulates amyloidogenic processing in lipid rafts. *J Neurosci*. 2013;33(27):11169-11183. doi:10.1523/JNEUROSCI.4704-12.2013

22. M J, R N. Interaction of peptides corresponding to fatty acylation sites in proteins with model membranes. *J Biol Chem*. 1995;270(28):16749-16755. doi:10.1074/JBC.270.28.16749

23. Yang X, Chatterjee V, Ma Y, Zheng E, Yuan SY. Protein Palmitoylation in Leukocyte Signaling and Function. *Front Cell Dev Biol*. 2020;0:1167. doi:10.3389/FCELL.2020.600368

24. Wan J, Roth AF, Bailey AO, Davis NG. Palmitoylated proteins: purification and identification. *Nat Protoc 2007 27*. 2007;2(7):1573-1584. doi:10.1038/nprot.2007.225

25. MT F, DT H, JW T, et al. Site-specific analysis of protein S-acylation by resin-assisted capture. *J Lipid Res*. 2011;52(2):393-398. doi:10.1194/JLR.D011106

26. BR M, BF C. Large-scale profiling of protein palmitoylation in mammalian cells. *Nat Methods*. 2009;6(2):135-138. doi:10.1038/NMETH.1293

27. Sanders SS, Martin DDO, Butland SL, et al. Curation of the Mammalian Palmitoylome Indicates a Pivotal Role for Palmitoylation in Diseases and Disorders of the Nervous System and Cancers. *PLoS Comput Biol*. 2015;11(8):1004405. doi:10.1371/JOURNAL.PCBI.1004405

28. M B, F D, L A, et al. SwissPalm: Protein Palmitoylation database. *F1000Research*. 2015;4. doi:10.12688/F1000RESEARCH.6464.1

29. M B, FPA D, FG van der G. SwissPalm 2: Protein S-Palmitoylation Database. *Methods Mol Biol*. 2019;2009:203-214. doi:10.1007/978-1-4939-9532-5_16

30. YX L, YH S, NY D. Improved prediction of palmitoylation sites using PWMs and SVM. *Protein Pept*

Lett. 2011;18(2):186-193. doi:10.2174/092986611794475084

31. W N, P J, Y G, et al. GPS-Palm: a deep learning-based graphic presentation system for the prediction of S-palmitoylation sites in proteins. *Brief Bioinform*. 2021;22(2):1836-1847. doi:10.1093/BIB/BBAA038

32. SL W, HJ K, CH H, TY L. MDD-Palm: Identification of protein S-palmitoylation sites with substrate motifs based on maximal dependence decomposition. *PLoS One*. 2017;12(6). doi:10.1371/JOURNAL.PONE.0179529

33. Reddy KD, Malipeddi J, Deforte S, et al. Physicochemical sequence characteristics that influence S-palmitoylation propensity. Published online 2016. doi:10.1080/07391102.2016.1217275

34. Adibekian A, Martin BR, Chang JW, et al. Characterization of a Selective, Reversible Inhibitor of Lysophospholipase 2 (LYPLA2). *Probe Reports from NIH Mol Libr Progr*. Published online 2010. Accessed August 19, 2021. http://www.ncbi.nlm.nih.gov/pubmed/24624468

35. A A, BR M, JW C, et al. Characterization of a Selective, Reversible Inhibitor of Lysophospholipase 1 (LYPLA1). Published online 2010. Accessed August 19, 2021. https://pubmed.ncbi.nlm.nih.gov/24624465/

36. FJ D, O R, N V, et al. Small-molecule inhibition of APT1 affects Ras localization and signaling. *Nat Chem Biol*. 2010;6(6):449-456. doi:10.1038/NCHEMBIO.362

37. RS K, BC D. Measuring S-Depalmitoylation Activity In Vitro and In Live Cells with Fluorescent Probes. *Methods Mol Biol*. 2019;2009:99-109. doi:10.1007/978-1-4939-9532-5_8

38. E L, GHH B. Spatial proteomics: a powerful discovery tool for cell biology. *Nat Rev Mol Cell Biol*. 2019;20(5):285-302. doi:10.1038/S41580-018-0094-Y

39. TP D, R W, JL G, P D, KS L. Localization of organelle proteins by isotope tagging (LOPIT). *Mol Cell Proteomics*. 2004;3(11):1128-1134. doi:10.1074/MCP.T400009-MCP200

40. CM M, LM B, A G, et al. Using hyperLOPIT to perform high-resolution mapping of the spatial proteome. *Nat Protoc*. 2017;12(6):1110-1135. doi:10.1038/NPROT.2017.026

41. A G, N KB, LM B, et al. Combining LOPIT with differential ultracentrifugation for high-resolution spatial proteomics. *Nat Commun*. 2019;10(1). doi:10.1038/S41467-018-08191-W

42. Itzhak DN, Tyanova S, Cox J, Borner GH. Global, quantitative and dynamic mapping of protein subcellular localization. *Elife*. 2016;5(JUN2016). doi:10.7554/ELIFE.16950

43. Itzhak DN, Davies C, Tyanova S, et al. A Mass Spectrometry-Based Approach for Mapping Protein Subcellular Localization Reveals the Spatial Proteome of Mouse Primary Neurons. *Cell Rep*. 2017;20(11):2706. doi:10.1016/J.CELREP.2017.08.063

44. N N, D R, MP S, et al. Putative glycosyltransferases and other plant Golgi apparatus proteins are revealed by LOPIT proteomics. *Plant Physiol*. 2012;160(2):1037-1051. doi:10.1104/PP.112.204263

45. Breckels LM, Mulvey CM, Lilley KS, Gatto L. A Bioconductor workflow for processing and analysing spatial proteomics data. *F1000Research*. 2016;5. doi:10.12688/F1000RESEARCH.10411.2

46. Itzhak DN, Schessner JP, Borner GHH. Dynamic Organellar Maps for Spatial Proteomics. *Curr*

Protoc Cell Biol. 2019;83(1):e81. doi:10.1002/CPCB.81

47. Garland M, Schulze CJ, Foe IT, Linden WA van der, Child MA, Bogyo M. Development of an activity-based probe for acyl-protein thioesterases. *PLoS One*. 2018;13(1). doi:10.1371/JOURNAL.PONE.0190255

48. Manna JD, Wepy JA, Hsu KL, Chang JW, Cravatt BF, Marnett LJ. Identification of the major prostaglandin glycerol ester hydrolase in human cancer cells. *J Biol Chem*. 2014;289(49):33741-33753. doi:10.1074/JBC.M114.582353

49. Hirano T, Kishi M, Sugimoto H, et al. Thioesterase activity and subcellular localization of acylprotein thioesterase 1/lysophospholipase 1. *Biochim Biophys Acta*. 2009;1791(8):797-805. doi:10.1016/J.BBALIP.2009.05.001

50. Kathayat RS, Cao Y, Elvira PD, et al. Active and dynamic mitochondrial S-depalmitoylation revealed by targeted fluorescent probes. *Nat Commun*. 2018;9(1). doi:10.1038/S41467-017-02655-1

51. Lin DTS, Conibear E. ABHD17 proteins are novel protein depalmitoylases that regulate N-Ras palmitate turnover and subcellular localization. *Elife*. 2015;4(DECEMBER2015). doi:10.7554/ELIFE.11306

52. Savitski MM, Zinn N, Faelth-Savitski M, et al. Multiplexed Proteome Dynamics Profiling Reveals Mechanisms Controlling Protein Homeostasis. *Cell*. 2018;173(1):260. doi:10.1016/J.CELL.2018.02.030

53. Zecha J, Meng C, Zolg DP, Samaras P, Wilhelm M, Kuster B. Peptide level turnover measurements enable the study of proteoform dynamics. *Mol Cell Proteomics*. 2018;17(5):974-992. doi:10.1074/MCP.RA118.000583/ATTACHMENT/63F48240-D18E-43CA-9390-AD879F6C69A8/MMC1.ZIP

54. Welle KA, Zhang T, Hryhorenko JR, Shen S, Qu J, Ghaemmaghami S. Time-resolved analysis of proteome dynamics by tandem mass tags and stable isotope labeling in cell culture (TMT-SILAC) Hyperplexing. *Mol Cell Proteomics*. 2016;15(12):3551-3563. doi:10.1074/MCP.M116.063230/ATTACHMENT/AC538293-0288-4F45-83EB-CAF62EBEAE5E/MMC1.ZIP

55. Dephoure N, Gygi SP. Hyperplexing: A Method for Higher-Order Multiplexed Quantitative Proteomics Provides a Map of the Dynamic Response to Rapamycin in Yeast. *Sci Signal*. 2012;5(217):rs2. doi:10.1126/SCISIGNAL.2002548

56. Ting L, Rad R, Gygi SP, Haas W. MS3 eliminates ratio distortion in isobaric labeling-based multiplexed quantitative proteomics. *Nat Methods*. 2011;8(11):937. doi:10.1038/NMETH.1714

57. Tan DJL, Dvinge H, Christoforou A, Bertone P, Arias AM, Lilley KS. Mapping organelle proteins and protein complexes in Drosophila melanogaster. *J Proteome Res*. 2009;8(6):2667-2678. doi:10.1021/PR800866N/SUPPL_FILE/PR800866N_SI_013.PDF

58. Orre LM, Vesterlund M, Pan Y, et al. SubCellBarCode: Proteome-wide Mapping of Protein Localization and Relocalization. *Mol Cell*. 2019;73(1):166-182.e7. doi:10.1016/J.MOLCEL.2018.11.035

59. Kennedy MA, Hofstadter WA, Cristea IM. TRANSPIRE: A Computational Pipeline to Elucidate

Intracellular Protein Movements from Spatial Proteomics Data Sets. *J Am Soc Mass Spectrom*. 2020;31(7):1422. doi:10.1021/JASMS.0C00033

60. Borner GHH, Hein MY, Hirst J, Edgar JR, Mann M, Robinson MS. Fractionation profiling: a fast and versatile approach for mapping vesicle proteomes and protein–protein interactions. *Mol Biol Cell*. 2014;25(20):3178. doi:10.1091/MBC.E14-07-1198

61. Szklarczyk D, Gable AL, Lyon D, et al. STRING v11: Protein-protein association networks with increased coverage, supporting functional discovery in genome-wide experimental datasets. *Nucleic Acids Res*. 2019;47(D1):D607-D613. doi:10.1093/NAR/GKY1131

62. Shu L, Hu C, Xu M, et al. ATAD3B is a mitophagy receptor mediating clearance of oxidative stress-induced damaged mitochondrial DNA. *EMBO J*. 2021;40(8):e106283. doi:10.15252/EMBJ.2020106283

63. Miranda S, Foncea R, Guerrero J, Leighton F. Oxidative Stress and Upregulation of Mitochondrial Biogenesis Genes in Mitochondrial DNA-Depleted HeLa Cells. *Biochem Biophys Res Commun*. 1999;258(1):44-49. doi:10.1006/BBRC.1999.0580

64. Zhang X, Ren D, Guo L, et al. Thymosin beta 10 is a key regulator of tumorigenesis and metastasis and a novel serum marker in breast cancer. *Breast Cancer Res*. 2017;19(1):1-15. doi:10.1186/S13058-016-0785-2/FIGURES/6

65. Sribenja S, Li M, Wongkham S, Wongkham C, Yao Q, Chen C. Advances in Thymosin β10 Research: Differential Expression, Molecular Mechanisms, and Clinical Implications in Cancer and Other Conditions. *https://doi.org/103109/07357900902849640*. 2009;27(10):1016-1022. doi:10.3109/07357900902849640

66. Vareli K, Frangou-Lazaridis M, Van Der Kraan I, Tsolas O, Van Driel R. Nuclear distribution of prothymosin alpha and parathymosin: evidence that prothymosin alpha is associated with RNA synthesis processing and parathymosin with early DNA replication. *Exp Cell Res*. 2000;257(1):152-161. doi:10.1006/EXCR.2000.4857

67. Brand IA, Heinickel A, Soling HD. Localization of a 11.5 kDa Zn(2+)-binding protein (parathymosin) in different rat tissues. Cell type-specific distribution between cytosolic and nuclear compartment. *Eur J Cell Biol*. 1991;54(1):157-165. Accessed November 26, 2021. https://europepmc.org/article/med/2032546

68. Havugimana PC, Hart GT, Nepusz T, et al. A census of human soluble protein complexes. *Cell*. 2012;150(5):1068-1081. doi:10.1016/J.CELL.2012.08.011

69. Marcon E, Ni Z, Pu S, et al. Human-chromatin-related protein interactions identify a demethylase complex required for chromosome segregation. *Cell Rep*. 2014;8(1):297-310. doi:10.1016/J.CELREP.2014.05.050